UNIVERSITA' DEGLI STUDI DI MILANO BICOCCA
Doctorate School of Science
Ph.D. in Physics and Astronomy

XXII CICLO

Plasma Treatment for Biomedical Application on Polymeric Substrate

Supervisor: Prof. Claudia Riccardi
Coordinator of the PhD school: Prof. Claudio Destri

PhD dissertation of: Roberto Ziano
Matr. N. 708227
PACS: 52.77.-j, 81.15.Gh, 87.55.jj

Abstract

This work arises from the possibility of changing the surface properties of materials with the use of plasma. It proved to be a very good method for treating surfaces, it is in fact able to modify surface properties of materials without altering their bulk properties. In particular, with the Plasma Enhanced Chemical Vapour Deposition (PECVD) is feasible sustaining the polymerization of a specific monomer depositing thin films containing interesting chemical groups. For these reasons, this technique was chosen for modifying polypropylene substrates through the polymerization of acrylic acid, an organic acid carrying the carboxy group (COOH). This chemical group is of particular interest because it has biocompatibility properties itself and can be used for a further grafting reaction allowing further surface modifications.

During this works two types of plasma reactor were optimized for obtaining the best working condition, namely, creating a stable coating of poly-acrylic acid resistant to Phosphate Buffer Saline (PBS) and water washing.

The physical and chemical properties of the deposited thin films were studied by means of Fourier Transform Infrared Attenuated Total Reflectance (FTIR-ATR), Water Contact Angle (WCA), X-Ray Photoelectron Spectroscopy (XPS), Atomic Force Microscope (AFM). The density of COOH groups into the polypropylene surface were evaluated by ion-exchange reaction with Thionin Acetate (THA).

A simple model for explaining the particular physical composition and stratification of the films is presented along with a computer simulation. The reactor geometry effect onto the film properties was also investigated. Furthermore, some applications of the process were discussed.

Part of the present work consisted in the use of the AFM for internal scopes and extramural collaborations. Among these, the measurement

of the thickness of different PEG chains bounded to the plasma treated surface in support of Monte Carlo simulations of their polymer dynamics.

Chapter 1

The Plasma State

1.1 Introduction

Plasma is usually called the fourth state of matter but it is not something we usually deal with, except for flames or a neon lights.

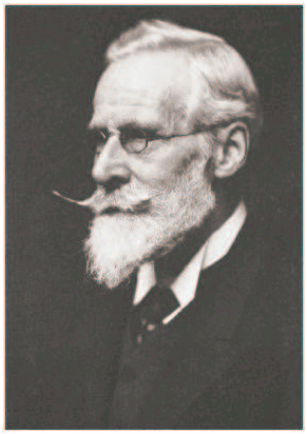

Figure 1.1: William Croockes (1832-1919)

The first experimental evidence of plasma (fig.1.5) into a laboratory was made by William Croockes in 1879, he called it "radiant matter". He was a pioneer in the construction and use of vacuum tubes for the study of physical phenomena. He was, as a consequence, one of the first scientists to investigate what are now called plasmas. The study of this state of matter remained only something curious since fifties when nuclear fusion was correlated to the study of plasmas with the possibility of energy production. Since then plasma began to gain interest.

Croockes also invented the famous radiometer whose mechanism of

working[1] has historically been a cause of much scientific debate. The explanation of the phenomenon was given by Osborne Reynolds (famous for the Reynolds number) only in 1879.

The nature of the Crookes tube was subsequently identified by British physicist Sir J.J. Thomson in 1897, and dubbed "plasma" by Irving Langmuir in 1928, perhaps because it reminded him of a blood plasma. Langmuir wrote: *"Except near the electrodes, where there are sheaths containing very few electrons, the ionized gas contains ions and electrons in about equal numbers so that the resultant space charge is very small. We shall use the name plasma to describe this region containing balanced charges of ions and electrons"*.

A quick introduction to the main characteristics of a plasma is necessary for further understanding and classification of plasma treatments.

A plasma can be qualitatively defined as: "a *quasineutral* gas of charged and neutral particles which exhibits a *collective behavior*" [1]. Quasineutral means that the plasma is neutral enough so that it is possible to approximate the density of negative charges with the density of the positive charges but not so neutral that all the interesting electromagnetic forces vanish. The collective behavior is related to the fact that local concentration of charged particles can generate long range Coulomb forces giving rise to strong local electric fields affecting the motion of the other particles.

A quantitative definition of what a plasma is can be done using the Saha law that furnishes the number of ionized atom expected in a thermal equilibrium gas:

$$\frac{n_+^2}{n_n} \simeq \frac{2}{\Lambda^3} e^{-\frac{U_i}{K_B T}} \tag{1.1}$$

$$\Lambda = \frac{h}{\sqrt{2\pi m_e k_B T}} \tag{1.2}$$

where n_n represents the density of neutral atoms, n_+ that of the ions, T the temperature of the gas and U_i the first ionization energy, Λ the

[1] Appendix A

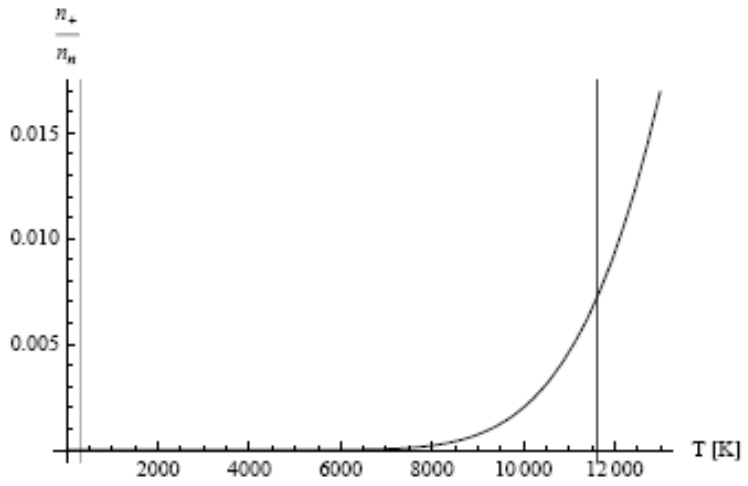

Figure 1.2: This image shows the relationship between the ratio between the densities of ionized atoms and neutral atoms in the case of the air at varying temperature. The vertical grey line identifies the ambient temperature, the black line, the typical temperature of a plasma ($11600\,K$).

thermal De Broglie wavelength, m_e the electron mass, k_B the Boltzmann constant and h the Planck constant.

Considering the air temperature at $300\,K$ and $U_i \approx 14\,eV$, the ratio of ionized atoms with respect to the neutral equals $n_+/n_n \simeq 10^{-122}$, a insufficient value for the generation of a plasma.

In Figure 1.2 it can be seen how changes the ratio of ionized and neutral atoms with temperature in the case of air. Increasing temperature, the ratio n_+/n_n is not relevant but when the k_BT becomes comparable to the first ionization energy, a further increasing of the temperature leads to the plasma state. This generally occurs at temperatures of the order of thousands of Kelvin degrees (in Figure 1.2 about 8000K).

In Saha's law, it is possible to notice that the ratio ionized-atoms/neutral-atoms has a strong temperature dependence. This is due to the fact that an atom becomes ionized when, colliding with another atom that has a sufficient amount of thermal energy, looses one or more electrons. In a

cold gas, only a small fraction of atoms have enough energy for this to happen.

1.1.1 Fundamental parameters

A full description of many charged particles system needs to specify the fields (E and B) generated from the particles themselves, the position (x) and the speed (v) for any particle in the volume of interest. In these cases statistical description it is very useful. It allows describe the system through the distribution function $f(x, v, t)$ defined for each species particles j. Unfortunately, even the distribution function is often impossible to completely determine, but may be approximate by some of its moments. The moments of lower orders are related to fundamental parameters needed to characterize a plasma: the density n of particles and T the mean kinetic energy.

1.1.2 Distribution function momentum

Consider a single species of particles and a plasma homogeneous in space and constant in time, the distribution function will depend only by speed: $f(\vec{x}, \vec{v}, \vec{t}) = f(\vec{v})$. The moment of order k of the distribution is defined by:

$$\vec{M} = \int f(\vec{v})(\vec{v})^k d\vec{v}$$

where, in general, $\vec{M}$ is a tensor of order k. For complete determination of $f(\vec{v})$ this tensor should be known for every k. The zero order momentum is a scalar quantity, which is simply the density of particles:

$$\vec{M}^0 = \int f(\vec{v}) d\vec{v} \equiv n$$

The first order momentum represent the average speed of particles

$$\frac{1}{n}\vec{M}^1 = \int f(\vec{v})(\vec{v}) d\vec{v} \equiv < \vec{v} >$$

The second momentum:

$$m \int (\vec{v} - < \vec{v} >)(\vec{v} - < \vec{v} >) f(\vec{v}) d\vec{v} = m[\vec{M}^2 - n < \vec{v} >< \vec{v} >] \equiv \vec{p}$$

where $\vec{p}$ is the pressure tensor. Since $\vec{p}$ is symmetric it exists a coordinate system that make it diagonal. In presence of a magnetic field, because of the trajectory of the plasma particles, the probability distribution function takes a rotational symmetry with respect to the field direction. So, the pressure tensor becomes:

$$\begin{vmatrix} p_\perp & 0 & 0 \\ 0 & p_\perp & 0 \\ 0 & 0 & p_\parallel \end{vmatrix}$$

If the distribution function is completely isotropic, $p_\perp = p_\parallel = p$ and temperature can be defined as

$$T = p/n$$

but in presence of magnetic field holds that $p_\perp \neq p_\parallel$, then is possible defining two temperature, one perpendicular $T_\perp$ and the other $T_\parallel$ parallel.

Relations among moments

So far we have considered only one species of particles, but in practice, the plasma has at least two species: ions and electrons. Often it is also necessary keeping in consideration the neutral and various types of ions. The moments can be separately defined for each species, this leads to different values of density and temperature and to a description at multi fluids.

Consider the case of a simple plasma, that is, composed only by electrons and ions with charge equal to Ze^4. The charge density is $e(-n_e + Zn_+)$. If n_e was different from Zn_+, then there would be a disequilibrium of charges and the consequent generated electrical field

would reestablish the equilibrium. This is the so called "quasi neutrality":

$$n_e \approx Z n_+$$

This is just the first of the three conditions which characterize the state of plasma. The previous relation correlates the zero order moments distributions of electrons and ions. The relationship among the first order moments:

$$\vec{j} = Z n_+ e < \vec{v_+} > - n_e e < \vec{v_e} > \approx n_e e(< \vec{v_+} > - < \vec{v_e} >)$$

Latter formula shows that the first order moments are linked, through electromagnetic fields, since the current density j is related to $\vec{E}$ and $\vec{B}$ through Ampere's law.

Generally the pressure and temperature of different species are not strongly coupled. Collisional processes that cause the transfer energy among different species are often slow compared to other energy transfer mechanisms. For this reason, the electronic and ion temperature are usually measured as distinct. In many cases it is often possible treat the plasma as if it were a single conductor fluid, in this case, the pressure is the sum of the pressures.

1.1.3 Characteristic parameters of plasma

As discussed in the previous section, starting with the basic parameters you can derive a number of other parameters that allow not only to characterize more exactly the type of plasma, but also a set of phenomena peculiar to this state of matter: for these reasons are defined characteristic.

Debye length

All plasmas are characterized by a length scale determined by temperature and density of its charged particles.

Suppose to place a test charge $-q$ in a homogeneous plasma. Immediately, the electrons are repelled and ions attracted. Result displacement of charges produces a local charge polarization shielding the rest of the plasma from the test charge. The characteristic length of this screen effect is called the Debye length.

Consider a uniform plasma of electrons and ions, and suppose that ions do not move and that electrons have a distribution function such that its density can be determined by the Boltzmann factor:

$$n_e = n_\infty e^{eV/K_B T_e} \tag{1.3}$$

where n_∞ is the electronic density at infinite distance form the test charge where potential is supposed to be negligible. After the positioning of the test charge and the equilibrium state is reached, the electrostatic potential V is given by Poisson equation:

$$\nabla^2 V = -\frac{\rho_q}{\epsilon_0} = -\frac{e}{\epsilon_0}(n_+ - n_e) \tag{1.4}$$

where ρ_q is the test charge density. Substituting 1.4 in 1.3 leads to:

$$\nabla^2 V = \frac{-e}{\epsilon_0} n_\infty \left[1 - \exp \frac{eV}{k_B T_e}\right] \tag{1.5}$$

in one dimension the solution is:

$$V \propto exp\left(\pm \frac{x}{\lambda_D}\right) \tag{1.6}$$

and with a further substitution of 1.6 into 1.5

$$\lambda_D = \sqrt{\frac{\epsilon_0 k_B T_e}{n_\infty e^2}} \tag{1.7}$$

The constant of proportionality can be determined by requiring that the solution is reduced to Coulomb potential when the distance x tends to zero. The complete solution is then:

$$V(x) = \frac{1}{4\pi\epsilon_0} \frac{q}{x} e^{-x/\lambda_D} \tag{1.8}$$

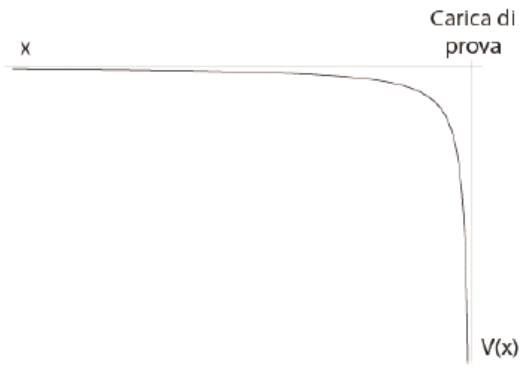

Figure 1.3: Debye-Hückel potential against distance from a test charge

The expression for the potential in 1.8 is known as *Bebye-Hückel Potential*. In fig 1.3 the Debye-Hückel potential is plotted against distance from a test charge.

A practical formula for a rough calculation of Debye length is:

$$\lambda_D = 6.9\sqrt{T_e/n_\infty}\, cm \tag{1.9}$$

where T_e is in kelvin and n_∞ is cm^{-3}.

Thanks to the Debye length it is possible to reformulate the condition of quasi-neutrality. It means that the plasma system size L must be very greater than the Debye length λ_D. If a non homogeneous charge distribution or an external potential were created into the plasma, they would be screened in a distance smaller than the size of the system, thereby preventing the formation of an electric field in the plasma.

Debye sphere

The criterion of quasi-neutrality, $\lambda_D << L$, is valid only if there are a sufficient number of particles in the region of Debye screen. This follows directly from the definition of Debye length which shows the dependence of λ_D from the density.

Let Define Debye sphere, the sphere that has the radius equal to the Debye length. The number of particles in this sphere is:

$$N_D = n_\infty \frac{4}{3}\pi\lambda_D^3 \tag{1.10}$$

The quasi-neutrality criterion can also be expressed through the following expression:

$$N_D >> 1 \tag{1.11}$$

1.1.4 Plasma frequency

If, in a uniform and homogeneous plasma, the electrons are moved from their equilibrium position, it creates an electric field. Latter originates a retraction force directly proportional to the displacement Δx given by Hooke's Law: $F = -kx$, where k is the elasticity constant of the "spring". The system behaves like a harmonic oscillator. The resulting oscillations are called *Langmuir Oscillations*.

Suppose that the plasma consists of a uniform region of electrons and fixed positive ions with density equal to that of electrons such as: $n_+ = n_e = n_0$. Suppose besides displacing the layer of electrons at a distance Δx, as shown in figure 1.4. There are three regions of charge:

- Region 1: net positive charge zone
- Region 2: neutral zone
- Region 3: net negative charge zone

in the region 2 the electrical field can be calculated using Gauss formula:

$$E = \frac{n_0 e \Delta x}{\epsilon_0} \tag{1.12}$$

Now, let the electrons move, it follows that:

$$m_e \frac{d^2\Delta x}{dt^2} = (-e)E = -\frac{n_0 e^2}{\epsilon_0}\Delta x \tag{1.13}$$

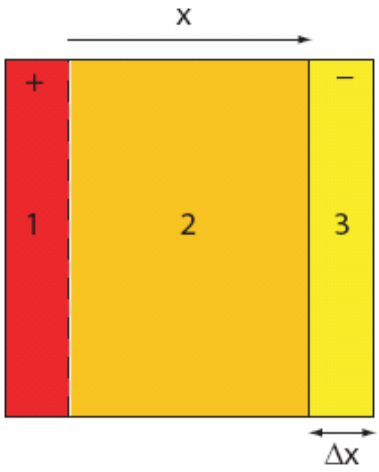

Figure 1.4: In this image, is shown schematically the displacement of a sheet of electrons (yellow) compared to a slab of ions (red).

that simplified lead to:

$$\frac{d^2\Delta x}{dt^2} + \left(\frac{n_0 e^2}{\epsilon_0 m_e}\right)\Delta x = 0 \tag{1.14}$$

The equation 1.14 is exactly the equation of an harmonic oscillator with resonance frequency equal to

$$\omega_{pe}^2 = \frac{n_0 e^2}{\epsilon_0 m_e} \tag{1.15}$$

that is called *electronic plasma frequency*. A simple and practical formula for calculating the plasma frequency is:

$$\nu_{pe} = 8980\sqrt{n_0}\, Hz \tag{1.16}$$

where n_0 is expressed in cm^{-3}.

If the plasma has more than one specie, every specie has its own plasma frequency

$$\omega_{pj}^2 = \frac{n_j q_j^2}{\epsilon_0 m_j} \tag{1.17}$$

where q_j is the charge of the considered specie.

it must, however, keep in mind that in a plasma with several species, they vary independently of each other, each with a proper frequency. Let consider only a plasma of ions and electrons, it can be shown that the plasma frequency is given by:

$$\omega_p = \sqrt{\omega_{pe}^2 + \omega_{p+}^2} \tag{1.18}$$

The plasma frequency, Debye length and thermal speed are related by:

$$\omega_{pj}\lambda_{D_j} = v_{T_j} \tag{1.19}$$

Cyclotron frequency

If a charged particle is injected in a uniform magnetic field, the Lorentz results force due to the uniform circular motion around a line of the magnetic field with a characteristic cyclotron frequency ω_c, is given by:

$$\omega_{cj} = \frac{q_j B}{m_j} \tag{1.20}$$

where q_j is the charge of every specie j.

A rapid way to calculate the electronic cyclotron frequency is using the following expression:

$$\omega_{ce} = 28B\, Hz \tag{1.21}$$

where the magnetic field has to be expressed in Tesla.

1.1.5 Plasma in the universe

In the universe there is a vast variety of plasmas, which are characterized for their basic parameters. Principally, plasmas can be divided into two broad categories: natural and artificial plasmas.

Natural plasmas: according to recent estimates the 99% of visible matter in the universe is in a plasma state [2, 3]. This includes the sun, most stars, nebulae and a significant part of the interstellar medium.

Earth's atmosphere, low temperature and high pressure are not favorable to the formation of plasmas, except in some special conditions. Common plasmas are the lightning and the ionosphere. Less common are other visible phenomena on the Earth like: the globular lightning and the Aurora Borealis.

Artificial plasmas: it is possible artificially producing a large number of plasmas with very different characteristics from each other. Plasmas are created for research purposes, for the study of thermonuclear fusion or processing of materials, mainly for industry. There are also that are not used for research, for instance, plasma televisions.

1.2 Cold Plasmas

Temperature is given by the thermal motion of the particles composing the plasma, in particular the ions. There are three types of particles: the positively charged, the negatively charged and the neutral ones and can have different equilibrium temperatures. When one says cold plasma one refers to the temperature of the ions, so the ions are slow respect to the electrons whose temperature can be very high. For instance a fluorescent light bulb is about $20{\cdot}000\,K$ but the density is less than that of a gas at atmospheric pressure, and the total amount of heat transferred to the wall by the electrons striking it at their thermal velocity is not that large.

The graph in fig. 1.5 gives an idea of the various types of known plasmas.

Let us focus on the so called cold plasmas. The condition of cold plasma is technically realized when the following criteria are matched [5]:

- the electrons are not in thermal equilibrium with the ions, which have a temperature not exceeding room temperature
- the plasma is weakly ionized

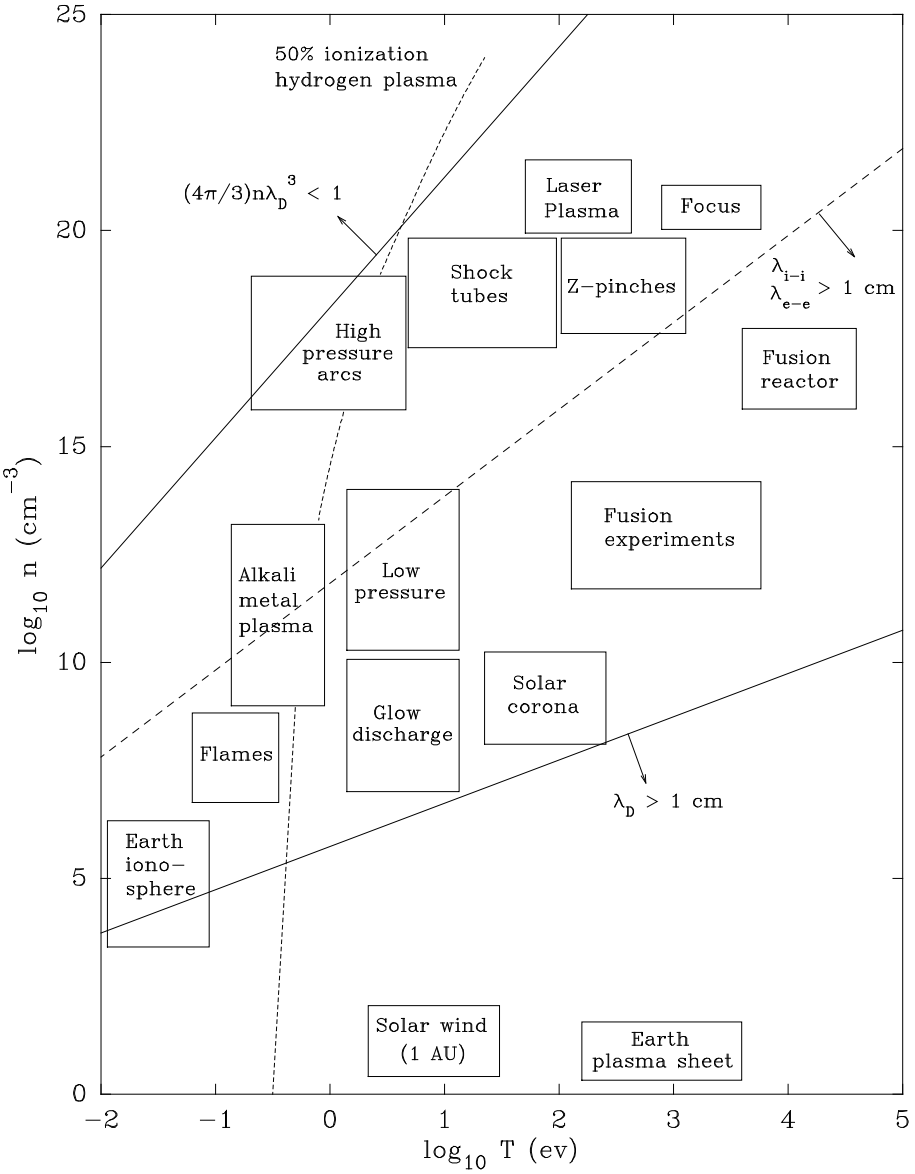

Figure 1.5: Different plasmas: plasma density (n), the total number of charged particles, versus temperature (T) [4].

- charged particles collisions with neutral gas molecules are important
- ionization of neutrals sustain the plasma in the steady state

Cold plasma occupies only a narrow band of energies in the graph describing all the known plasmas in nature, but are largely employed for the modification of surface properties of materials. Plasma technologies have a great importance in several industrial fields for the optical, physical, and chemical modifications of materials surface. For example about one-third of the processes needed to make a modern semiconductor chip involve a plasma-based process. Indeed, materials and surface structures can be fabricated that are not attainable by any other method, and the surface properties modifications are unique.

There are many different way to produce a cold plasma for surface treatments, at first a big difference can be done between atmospheric plasmas and low pressure plasmas. Among the low pressure ones there are the capacitively coupled or inductively coupled reactors, also very diffuse are the microwave plasma reactors. Instead, among the atmospheric pressure ones there are dielectric barrier discharge (DBD), plasma jet and coronas. The discharge inside the reactor can be powered by a radio frequency generator or by a constant voltage, moreover, the power source can be a pulsed or a continuous wave.

During the latest years there was an increasing interest in plasma processes at atmospheric pressure. These types of processes are easy to implement in a chain of production where, for instance, a roll to roll system is required or where hight manufacturing speed is needed.

On the contrary low pressure plasma treatment are slower, more expensive because they need vacuum chambers pumping systems that increase the production costs that do not like to manufacturers.

As already exposed, atmospheric pressure plasma are more attractive from the manufacturer point of view but they have some limits. In fact,

with respect to the uniform thin film deposition, an homogeneous discharge is the key parameter that in practise is very difficult obtaining through in an atmospheric Discharge [6].

1.3 Plasma Surface Interaction

In a typical reactive plasma the gas phase chemistry is extremely complex because the highly energetic electrons can activate a great number of reactions. In a plasma the species include neutral atoms and molecules, positive and negative ions, radicals, electrons and photons. These species interact with the surface of materials activating a number of processes which can be summarized as:

- **Activation**: generation of free radicals on the surface. The energy given by plasma can brake bonds between the atoms composing the surface of the samples making them ready to form a new bond with incoming molecules.

- **Etching**: chemical or physical ablation of the material surface. Atoms, molecules and ions that impact onto the exposed surface of the sample can remove material. This process enlarge the surfaces roughness as well as its area.

- **Deposition**: deposition of a thin film on the surface. The film can be produced adding molecules at the plasma phase. The plasma is able to open some bonds of the molecules that ready for a new one approach the surface. During this period they are able to recombine with other molecules or radicals both in the plasma phase and onto the surface. This process create a solid growing film upon the substrate surface

- **Grafting**: reaction of chemical groups insertion. When an ion, a molecule or a radical reaches the surface where there is an active

site, they can chemically react to form a bond with the atoms of the surface to reduce their total energy. When polar groups are grafted to the surface, the process improves surface adhesion.

Often in reactive plasmas all of the cited processes are present, thus the knowledge both of the gas-phase and surface chemistry is fundamental for the development of plasma applications.

Among the several uses of a plasma (cleaning surfaces, cutting, milling, etc.) there are: plasma treatment and plasma polymerization. The plasma treatment of materials utilize gases such as Ar, N_2, O_2, NH_3, and CF_4 to insert or substitute chemical functionalities onto a substrate or to create radicals for crosslinking or subsequent surface grafting. Plasma polymerization involves the fragmentation and subsequent deposition of organic monomers, some etching can also occurs simultaneously as a result of the bombardment of both the substrate and the growing coating by ions as well as from Vacuum Ultra Violet (VUV) radiation. Depending on various factors such as the process vapour, substrates and process conditions, deposition, substitution or etching can dominate in modifications on the materials surface. All the above described processes deal with the interaction of the chemical species with the surface.

Surface reaction mechanism for most plasma processes are still not well understood and characterized. However, adsorption and desorption of reactive species on the surface are usually part of the complex surface processes. *Adsorption* is the mechanism that brings an atom (or molecule) to form a stable bond with the surface. There are two kinds of adsorption processes: *physisorption*, which is the creation of a bound due to the weak attractive Van der Waals forces between the atom and the surface, and *chemisorption* which is due to the formation of a chemical bond between the atom (or molecule) and the surface. Chemisorption is an important process, when a chemical bounds are formed they increase the stability of the deposition, a property needed for quite all applications. These two kinds of adsorption mechanisms are often found in the

same system with different regimes favored depending on surface temperature and chemical environment. *Desorption* is the reverse reaction to adsorption and, in thermal equilibrium, the two reactions must be balanced.

Along with the described processes, in a typical reactive gas a wide variety of chemical reactions are to be considered in the gas-phase chemical equilibrium. The radical production processes are responsible for the creation of extremely reactive species that can interact with other elements of the atmosphere or on the surface. These species are usually extremely important for plasma processing. Usually the number of these reactions is very high and the complete description of the chemical equilibrium of a reactive plasma can become an overwhelming task.

1.4 Plasma enhanced chemical vapour deposition

A special role in the surface functionalization (and also in this thesis work) is covered by Plasma Enhanced Chemical Vapour Deposition (PECVD) of functional polymers [7, 8, 9]. PECVD of polymers is also known as plasma polymerization. Plasma Polymerization is defined as the process that converts monomers precursors into polymers via the formation of the gas phase radicals and their recombination at radical sites during film growth.

By controlling the chemical composition of the plasma phase (gas precursors) and the plasma ignition parameters (power, pressure, electrodes configuration) it is possible to tune the complete spectrum of physicochemical properties of the deposited layers ranging from the chemical composition, the wettability, the mechanical properties etc.

Among the different cold plasmas used for materials processing PECVD is one of the most interesting techniques for obtaining functionalised surfaces for bio-applications.

The drawback is that plasma polymerization process is extremely complex from a microscopic point of view, since it involves different mass transport and diffusion processes, giving rise to non-homogeneous and non completely predictable chemical characteristics of the synthesized polymers. On the other hand the possibility to deposit ultra-thin ($< 10\,nm$) polymer functional layer whatever the substrate, makes plasma polymerization a very interesting techniques for many technological applications. From the macroscopic point of view the condition of operation of the plasma polymerization process can be well described by the Yasuda factor [10], defined as:

$$W/FM \tag{1.22}$$

Where W is the ignited power, F is the flow of the monomer and M is the monomer molecular weight. The parameter F defines two deposition regimes, known as the power deficient regime for low values of F and the monomer deficient regimes for high values of F. In the power deficient regimes the power available in the plasma phase is too low as compare with the amount of the monomer present, this result in the deposition of a polymer film with chemical properties very similar to the precursors but very poorly cross-linked, thus with very poor mechanical/chemical stability. In the monomer deficient regime, the power available for polymerization is abundantly enough for creating a stable polymer but with the composition much different from the precursors.

In this perspective, the study of plasma parameters in relation to the Yasuda factor is extremely important in order to obtain functional films also characterized by a good degree of stability, in particular in liquids.

In order to increase the degree of functionality and film stability, the pulsed discharge technique was introduced by Yasuda in 1977. In this method power is given to the plasma in pulses with a frequency much lower than the RF excitation frequency ($13.56\,MHz$). The parameter that characterizes pulsed plasmas is the pulse period and the duty cycle. The duty cycle is given as the ratio of the pulse ON time to the total

time period, defined as:

$$D = t_{on}/(t_{om} + t_{off}) \tag{1.23}$$

Resulting in an effective power described by:

$$P_{eff} = P_{on}D \tag{1.24}$$

Plasma polymerization occurs during the ON period and during the OFF time (usually $T_{off} > T_{on}$) radical chain propagation could take place hereby increasing retention of the functional group of the monomer in the deposited films. The use of low power additionally prevents excessive monomer fragmentation and reduce the plasma induced damage to the deposited polymers.

Chapter 2

Biocompatibility

2.1 Introduction and definitions

The definition of biocompatibility is controversial, not a single definition is given but a variety of concept can be listed as follow:

- The ability of a material to perform with an appropriate host response in a specific application. [11]
- The exploitation by materials of the proteins and cells of the body to meet a specific performance goal. [12]

The first definition, the oldest, is very vague, since biocompatibility is defined according to the application. It does not offer useful insight into what materials are biocompatible, how they work or how to design improved materials.

The second definition tries to better specify this concept, it suggests the central role of interfacial proteins and cellular recognition processes in biocompatibility while also stressing the active role of the biomaterials.

Anti-fouling can be a properties of biocompatibility, it is in fact a specific behaviour of the material when put in contact with proteins. The anti-fouling is a properties of a material to limit totally or in part the

protein from sticking on it. In fact protein are the first agent to come in contact with en extra body object, to stick on it and to denature, opening the way to successive reject of the object by the body. Also fouling can be listed among the biocompatibility properties, in this case the material interact with cells improving their sticking. For instance the ability to improve cell growth is considered a biocompatibility properties. Especially in contact with blood, compatibility means that no coagulation takes place [13]. Materials that exploit the biological environment to lead to degradation or to resist degradation are considered biocompatible even if they behave in an opposite way.

For instance, biocompatibility refers to the fact that a prosthesis or a biomedical device in non-toxic, performs properly the function it was engineered for, and is tolerated by the biological district where it is "at work" for a reasonable period of time [14].

One of key issue for biocompatible surfaces development is the control of the immobilization of the biomolecules on the surface. To address this problem, the attention of the researchers has been devoted on the biological aspects (i.e. the molecular structure of the protein and how it influences the mechanism of recognition) as well as to the surface engineering aspect (i.e. the control of the surface physico-chemical properties).

2.2 Surface functionalization techniques

Attaching bioactive compound can be further step in biocompatibility because it allows changing the properties of a surface with that of the active compound. Surface modification techniques must be tailored to introduce a specific functional group which will be used for the immobilization.

Surface functionalization techniques can also modify surface properties by introducing random, non specific groups or by coating non-specifically the surface. There are several surface functionalization tech-

niques developed during the last decades which can be classified in terms of the production of chemically pure and controlled surfaces, their physical properties (such as roughness), the flexibility (i.e. the need of a specific substrate) but also in terms of their production aspects (waste production or use of hazardous materials).

In the following subsections two main classifications of the surface functionalization techniques will be briefly described, the wet and the dry chemical techniques.

2.2.1 Wet chemical techniques

In wet chemical based techniques, a material is exposed to liquid reagents in order to generate reactive functional groups on the surface. One of the most important technique in this category is the use of the Self-assembled-monolayers (SAMs) on specific substrates. It consists in the self assembly of a monolayer of a particular class of molecules on an suitable substrate. Among the numerous combinations, we will briefly describe the two most commonly used:

- Thiolated molecules (alkyl thiols) on gold and other noble molecules [15]
- Organosilanes on Silicon and Silica [16]

SAMs are easy to fabricate, may have many types of head groups and are therefore convenient, flexible, and simple means for functionalizing a surface. Nevertheless SAMs surface coverage depends on the surface properties and cleanness. Also they tend to oxidize under ambient conditions after a few hours. Another wet chemical based technique is the electrodeposition: in summary a conductive is used as a counter electrode in an electrochemical cell containing the precursor of the polymer that has to be deposited, dissolved in an electrolyte. Many examples in literature have shown that this techniques is able to produce polymeric

thin films with special biofunctionalities [17]. This technique is very useful for the productions of thick coatings since it is possible to obtain very high deposition rates. On the other hand its use is limited to conductive substrates.

Within the wet chemical techniques, a special role is played by the modification of surfaces by hydro gels. Also in this case many functionalities can be produced.

Among other wet techniques we can cite spin coating, dip coating and Langmuir-Blodgett [18]. The principal advantage of those techniques with respects to SAMs and electrodeposition is that no specific substrate is needed. The disadvantage is that they require large amounts of chemicals and it is possible to coat flat substrates only.

2.2.2 Dry chemical techniques

Among the dry chemical techniques a major role is covered by plasma based processes [19]. Plasma processes are used since many decades and offer unique advantages for many technological applications such as micro and nanofabrication.

Plasma based functionalization techniques has the advantage to allow the modification and the control of a wide spectrum of surface properties of the materials such as chemical composition, wettability, adhesion, hardness, refractive index, etc. or to enhance the deposition of thin films on a solid surface. The main advantages of plasma techniques for biorelevant surface functionalization are:

- Plasma physics and chemical principles are well understood since a long time and this base knowledge can be exploited for other applications.

- Plasma engineering is usually reproducible, reliable and especially applicable to different sample geometries as well as different materials such as metals, polymers, ceramics and composites. More-

over, a major advantage is that plasma process can be operated at low temperatures making them applicable to thermo-sensitive substrates.

- Plasma processes can be monitored accurately using in situ in the plasma diagnostic devices.
- Plasma processes can provide sterile surfaces and can be scaled up to industrial application production.
- Plasma techniques are compatible with masking and lithography techniques to produce surface patterning.

The type of functionalization obtained can be varied by the selection of the gas of the discharge (Ar, N2, O2, H2O, CO2, NH3) and operating parameters (pressure, power, time, gas flow rate). Oxygen plasma is often used to create oxygen containing functional groups and polymer surfaces. Ammonia and nitrogen plasmas have been used to graft amine groups to the surface. Inert gases can be used to introduce radical sites on the polymer surface for the subsequent graft copolymerization.

2.3 Materials

Polymeric materials like Polypropylene (PP) are widely used in many technological fields due to their suitable bulk properties, easy workability and low manufacturing costs. While maintaining the bulk properties of polymers, the plasma can tailor their surface properties for specific use. Thus, for many applications it is necessary to modify the surface of the polymers chemically, in order to enhance or change their properties, for instance, generating biofunctional surfaces. Vascular grafts, heart valves, catheters, intra oculars lenses and contact lenses are only a few examples of various applications in the biomedical field.

There is a growing demand of PP into the healthcare and surgical field for its mechanical (resistance to stress, sterilization, easy to style) and physical properties (relatively high meting point, non toxic). Many object are made by PP, among them there are syringes, gloves, catheters, membranes for filtration. All this products need to be biocompatible.

The specific intent of this work is functionalizing a polymeric material, like Polypropylene (PP), with active groups onto the surface for giving it biocompatibility properties.

2.4 Plasma and biocompatibility: state of the art

In order to functionalize surfaces, different types of functional groups could be chosen, the main chemically reactive groups amenable for covalent immobilization of biologically active molecules are: amine (NH_2), carboxy (COOH), hydroxy (OH) and aldehyde (C=O) [20].

Aldehyde surfaces cannot be produced by plasma treatments as plasma polymerizaton is necessary. However volatile aldehydes easily lose C=O reducing the efficiency and low power had to be used which reduces the deposition rates.

Hydroxy groups are less attractive than amines and carboxyls on account of their lesser nucleophilic character and hence lesser chemical reactivity. Reaction designed to target surface hydroxy groups can suffer from interference by water molecules.

Aminated surfaces have some problem related to the fact that carboxy groups of a protein to be immobilized can interact with amine on the same protein or another protein rather than amine on the surface, in fact when the carbodiimide activates the carboxy groups present on the protein, they can interact with amine groups of another protein before reaching the surface, causing crosslinks and oligomeric protein agglomerates. Such agglomerates become less soluble and can then adsorb on the

surface without a covalent bond and leading to a compromised biological function. It is better to turn the scheme around. Namely, to use carboxylated surface to react with amine groups on the protein. In this case it is possible to activate only the carboxy groups on the surface adding the proteins after the activation process. This guarantee the interaction of the surface carboxy groups only.

Carboxylated surfaces can be obtained via plasma treatment with CO_2 [21] but the density are not so large as for plasma polymerization.

Acrylic acid and propanoic acid [22] are used in plasma polymerization process. Acrylic acid, thanks to the presence of the double bond C=C, leads to radical grafting and its deposition rate is higher than that with propanoic acid. Surfaces functionalized with carboxy groups gain biocompatibility properties due to hydrophilic character of the COOH groups themselves (increase protein adsorption) and can be used for a post grafting with, for instance, bis-amino-terminated Poly(Ethylene Glycol) (PEG).

After a carefully analysis of advantages and disadvantages, the choice fell on carboxy groups through the plasma polymerization of acrylic acid.

The plasma polymerized Acrylic Acid (ppAAc) has been proven to provide highly functionalised surfaces. This kind of surface modification is suitable either to promote and control cellular growth [23, 24] and for immobilization of bioactive molecules both via electrostatic and/or covalent binding. With respect to this, one of the key issues in the deposition process is the stability of the film in biological fluids and in polar liquids (i.e. water).

The ability to withstand dissolution is important to prevent false negative results from the underlying substrate during cell adhesion or protein adsorption studies. Some researchers used co-polymerization of acrylic acid with other monomers such as octa-1,7-diene to prevents the dissolution of the plasma polymers by water [25].

Chapter 3

Experimental Apparatus

3.1 Reactors

The experimental apparatus is principally formed by two plasma reactors. The first one to be build was the reactor A, a capacitively coupled reactor that will be sharply presented in the following section. The second one was the reactor B, always a capacitively coupled reactor but with a different antenna configuration and shape. Also this reactor will be showed in details after reactor A. The very difference between the to reactor lays in the fact that the monomer, in the former case is forced passing through the antenna, where the RF is stronger and causes a great fragmentation of the monomer itself, instead in the latter case the monomer enters into the chamber of reaction and reaches the sample without the direct contact with the antenna. However, all that implies this basic difference will be discussed in the chapter.

3.1.1 Reactor A

The first reactor (fig. 3.1), a capacitively coupled radio frequency plasma reactor, is constituted by a cylindrical stainless steel vacuum chamber (diameter $30\,cm$) with two horizontal parallel plates that act as electrodes.

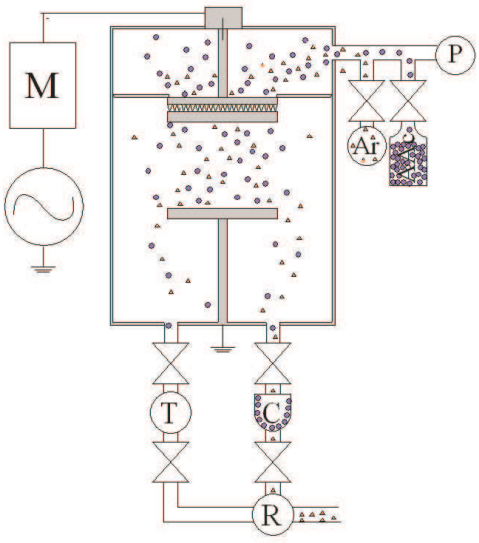

Figure 3.1: Reactor A

The plates are of 15 cm in diameter, placed at 4 cm far away from each other. The bottom electrode, used as samples holder is connected to the ground. The upper electrode is connected to the RF generator and acts as antenna. The gas mixture flows from the upper side through the above electrode shaped as a shower (pinholes diameter of 2 mm). The peculiar shape of the antenna assures that the feeding gas is uniformly spread into the chamber. A constant flow is guaranteed by a rotary pump (Varian SD-300). The powered electrode is externally connected, through a semi-automated matching network (Advanced Energy ATX-600), to a 13.56 MHz RF power supplier (Advanced Energy RFX-600) which provides an RF voltage with respect to the ground.

A picture in 3.2 shows the reactor during a treatment. The front window it is useful for checking the treatment and inserting and extracting samples from the chamber.

Figure 3.2: Picture of the reactor A running. Inside the chamber the typical azure glow of argon gas discharge is visible.

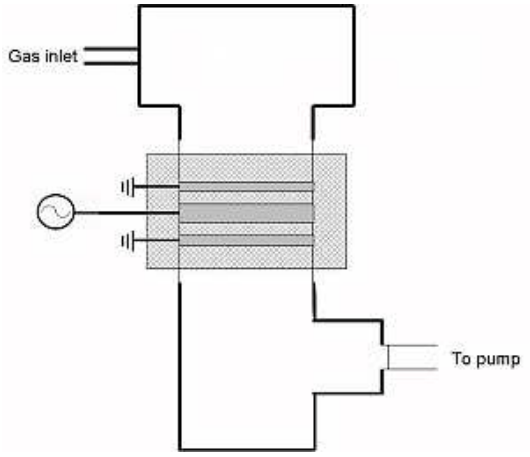

Figure 3.3: Reactor B

3.1.2 Reactor B

The second reactor (hereafter reactor B) is constituted by a cylindrical glass chamber (inner diameter $10\,cm$, length $30\,cm$), closed at each end with stainless steel flanges (fig. 3.3). An RF power supplier is connected through a matching network to a copper ring wrapped around the cylindrical chamber in the middle of the glass tube. Two other copper rings, placed apart from the RF antenna, are grounded. The samples are suspended between the ring acting as antenna and the grounded ones. Prior to the depositions, the reactor has been evacuated up to $10^{-1}\,Pa$ by means of a rotary pump. In both reactors the monomer is kept in a quartz flask connected to the reaction chamber by a needle valve instead the gas carrier is connected through a flow meter (EL-Flow series F-201C by Bronkhorst). The Acrylic Acid (AAc) reservoir is maintained at room temperature by immersion into a water bath.

For both reactors, the AAc acid flow was measured making the difference between the weight of the acid flask before and after every treatments, while the carrier gas flow was measured directly through the flow meter. Main differences form reactor A are, the different path that the

Figure 3.4: Picture of the reactor B

gas and the monomer have to follow inside the reactor before reaching the sample, as already underlined, the volume of B is lower with respect to A and the materials, stainless steel versus quartz. All these characteristics influences the discharge and the effects of the treatments on the materials.

Either rector are equipped with a cold trap in order to prevent the monomer to reach the rotative pump and spoiling it. Moreover, the cold liquid nitrogen trap acts as a pump not only for the monomer but for water vapor, present in the air, too. This is useful for the evacuation of the chamber prior of every treatment, it is more efficient both for pumping speed and for types of element pumped.

3.2 Experimental Procedure

In order to obtain a thin film of polymer containing carboxy groups we chose to polymerize acrylic acid in a mixture with argon gas. This acid is the simplest unsaturated acid carrying the desired group, the molecular structure is presented in fig. 3.5. It is a planar molecule which molecular

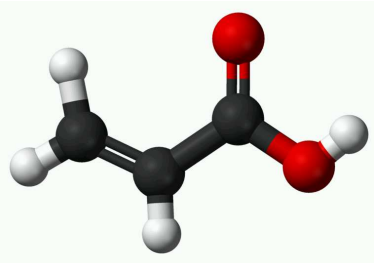

Figure 3.5: Structure of Acrylic acid molecule, oxygen atoms in red, carbon in black and hydrogen in withe colors. $M = 72.06\,g/mol$

formula is $C_3H_4O_2$.

Three different mixtures were tested:

1. A rich acrylic mixture, the ratio of acid flow against argon flow was 9:1 (AAc flow $9\,sccm$, Ar flow $1\,sccm$).

2. An equi molar mixture of acid and gas (AAc flow $3\,sccm$, Ar flow $3.3\,sccm$).

3. A poor acrylic mixture with a ratio of 1:2 (AAc flow $1.25\,sccm$, Ar flow $3.3\,sccm$).

The experiments were planned as follow:

- A set of treatments at varying Radio Frequency (RF) power input with fixed time, pressure, temperature and flows were carried out producing coated samples.

- The stability of the coatings were checked washing the samples in water and PBS for $24\,h$ at a controlled temperature of $37\,°C$. There are many data on the retention of COOH groups after plasma treatments but only few measure the retention after the washing in a water solution.

- The minimum power at which the coatings are stable was found out.
- The found minimum stability power was used in a new set of measurements at varying treatment time producing films with different thickness and crboxy groups.
- Analysis of the previous samples leads to the surface and volume densities of the active groups.

Samples of thin films of polypropylene were put on the lower plate of the reactor A after having cleaned them with acetone. The chamber was evacuated by a rotary pump (Varian SD-300) combined with a turbo-molecular pump (Leybold RS232) till a pressure of $10^{-4}\,Pa$ before refilling the reactor with argon gas at a typical pressure of $10\,Pa$. During the refilling process only the rotary pump was working. At the equilibrium conditions the gas flow was kept constant by the flow meter. Then the substrate was activated by $30\,sec$ plasma treatment in pure argon at $100\,W$ in reactor A.

In the reactor B samples were suspended inside the chamber in order to be positioned between the antenna and the two grounded rings. After having reached the equilibrium conditions, as in reactor A, the substrate was activated by $30\,sec$ plasma treatment at $40\,W$. The difference in the activation power is due to the different geometry. A bigger activation power in reactor B leads to a spoiling of the substrates.

After the activation stage, in both cases, the needle valve closing the acid flask was readily opened and the work went on till the end of the treatment.

3.3 Diagnostics

Films structures were determined by means of a Fourier Transform Infrared (FTIR) spectrometer (Nicolet Avatar 360) equipped with a PIKE

MIRacle Attenuated Total Reflectance (ATR) sampling accessory, suitable for the collection of spectra in the range between $400 - 4000\,cm^{-1}$. For each spectrum 32 scans, with a spectral resolution of $4\,cm^{-1}$, were recorded.

Hydrophilic characteristics of the treated samples were evaluated by means of static contact angle measurements (DataPhysics OCA 20 instrument).

Measurements with the Atomic Force Microscope (AFM) were carried out using a Solver P47-PRO (NT-MDT, Moscow, Russia), in semicontact (tapping) mode on dry samples using HA_NC (High Accuracy Non Contact) silicon tips (NT-MDT) of typical spring constant $5.8 \pm 1.2\,N/m$ and resonance frequency $200 \pm 20\,KHz$. Square images were collected at a typical frequency of $1.5\,Hz$ and with 256 points per line.

Measurements of the absolute number of active sites were performed by titration with the thioninacetate dye.

X-ray photoelectron spectra were recorded using a 5500-PHI (Physical Electronics) apparatus, with a monochromatic Al-anode $K\alpha$ source and an electron take-off angle of 68 degrees. The analyzed circular area had a diameter of $0.8\,mm$. The pressure in the chamber was roughly $10^{-6}\,Pa$. The spectrometer was calibrated by using the $Ag_3d_{5/2}$ peak and the resulting energetic resolution was $0.46\,eV$.

3.3.1 ATR-FTIR

The FTIR-ATR employs a total internal refracted ray of monochromatic light to measure the absorbance of a sample: the measure is the difference between the intensity of the reflected ray with and without the sample. The penetration depth of this ray depends on the incidence angle and the wavelength of light. The penetration depth can be expressed as: $d_p = \frac{\lambda_i}{2\pi\sqrt{(n_1 sin\theta_i)^2 - n_2^2}}$ where n_1 is the refractive index of the ATR crystal, n_2 is the refractive index of the sample, θ_i the angle of the incident ray with respect to the perpendicular to the crystal and λ the wavelength of

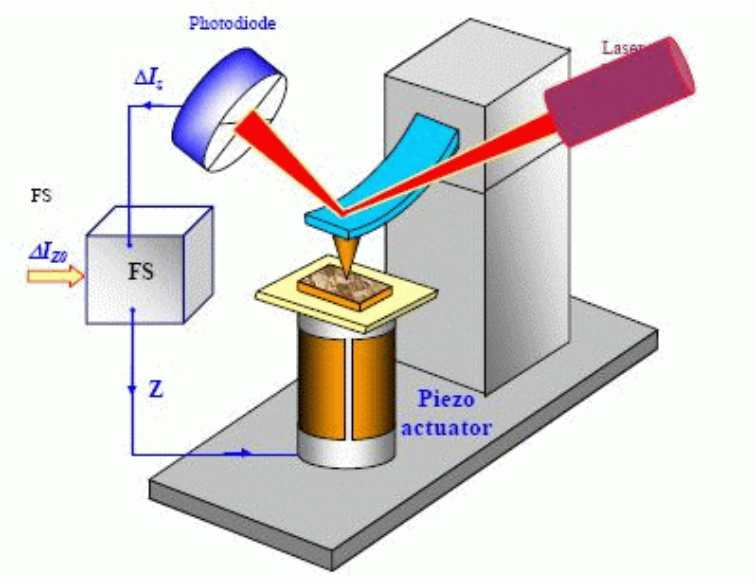

Figure 3.6: A scheme of AFM set up. This is a simple scheme but all the essential elements are pictured, the cantilever and tip, the piezoelectric actuator, the feedback system, the laser and photo detector and the sample.

the scanning ray. The ATR crystal made of Zinc Selenide (ZnSe) has a refractive index equal to 2.4 and the refractive index of the PP substrate is equal to 1.49. When the incidence angle is near to the critical angle (the angle of maximum penetration) the value of d_p can be approximated to one wavelength. At the light of the fact that the wavelengths analysed range from $4000\,cm^{-1}$ to $400\,cm^{-1}$, namely from $2.5\,\mu m$ to $25\,\mu m$, so is the penetration length. For instance, at $1000\,cm^{-1}$ with an incidence angle of 45° on a PP sample the penetration is of $1\,\mu m$.

3.3.2 AFM

The AFM is composed of a nanometric tip at the end of a cantilever that flexes itself when the tip comes in contact with the sample surface. A sensor measures the position of a laser spot reflected from the upper side

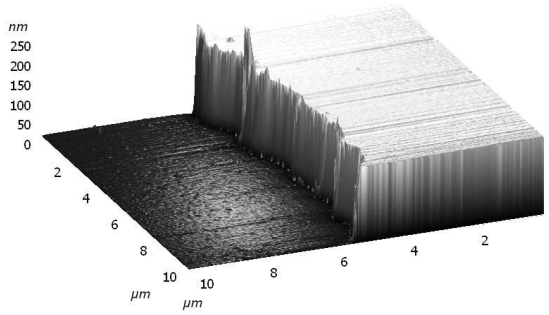

Figure 3.7: AFM image of a step left after removing the adhesive tape

of the cantilever. A piezoelectric device changes the relative position of cantilever (sample)with respect to the sample (cantilever tip) in order to maintain the position of the reflected spot constant. This means maintaining a constant force between tip and sample. The displacement of the piezoelectric corresponds to the relative height of the sample in that point. Repeating the procedure point per point and line per line, a matrix containing the relative heights of the sample is obtained. Converting the heights values in gray scale tones, it is possible to create an image of the sample surface. Usually the dark tones represent the bottom points while the brights, the higher ones.

The procedure jet described is usually called “constant force” or “contact” mode and the tip is in continuous contact wit the sample. There are other modality to perform an AFM measure. One very common is the so called “constant amplitude” or “semi contact” or “tapping” mode. This mode counts that the cantilever is kept in vibration at its resonant frequency by an external excitation modulating force. Approaching

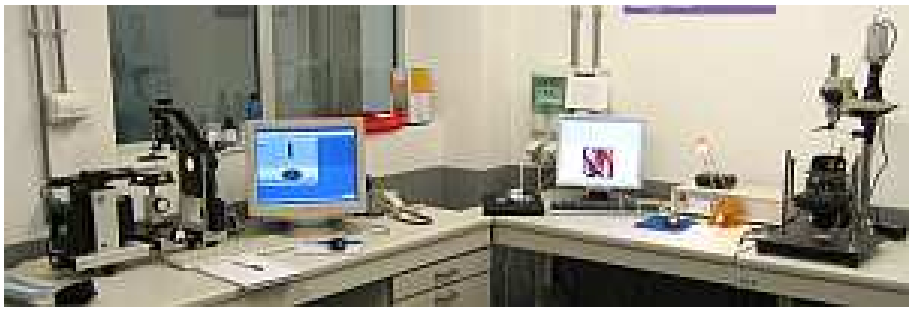

Figure 3.8: WCA on the left and AFM on the right

the sample, the cantilever modify its amplitude of vibration for Van der Waals long range interaction forces. In this case the feedback system tries to maintain the amplitude constant varying the relative position of cantilever and samples. Also in this case, repeating the procedure point by point and line by line, a matrix is collected and can be visualized as an gray scale image of the heights. In this modality, the tip is not in continuous contact with the sample but only for following instant. This is the preferred mode for soft sample and this is the modality used for all the measurements of this work. A simple scheme of the apparatus is presented in figure 3.6.

Thickness of the film for each different treatment power was measured by AFM on silicon wafers samples treated at the same time of the PP ones. Before treatment an adhesive tape was used to mask a portion of the silicon wafer. After treatments, adhesive mask was carefully removed leaving a step (fig. 3.7) because the masked portion do not experimented any deposition effect, and film thickness was measured.

This measurement was performed on silicon instead of PP because of the silicon flatness and stiffness. Profs were done on PP samples but after the remotion of the masking tape the PP surface resulted so altered that any measurements of the thickness was useless.

During the analysis, samples were mounted on a sapphire substrate,

using a 200 μm high double-sided tape (Tesa AG). Squares of different size (from 25 μm^2 to 1 μm^2) were scanned, and Nova SPM software (NT-MDT) was used for image corrections.

A picture of the Contact Angle (CA) and AFM instruments 3.8.

3.3.3 Thioninacetate labelling

Thioninacetate is a dye that interacts with the carboxy groups present into the deposited films, forming a bond. The amount of bonded dye is measure through a spectrometer. The measure of the intensity of the scattered ray is compared to a calibration curve obtained with solutions of thioninacetate at different concentrations leading to the total amount of dye in the film. The exact procedure is following described.

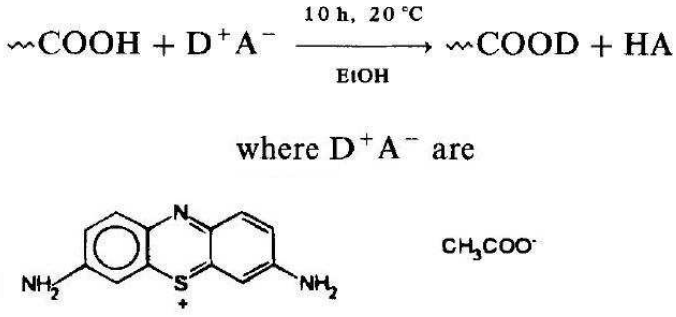

Figure 3.9: Reaction scheme of thioninacetate with carboxy group

Dishes of plasma coated PP (3 cm diameter) were immersed for 20 hours in a 0.1 g/l solution of the dye in a mixture of water and ethanol (1:1). In fig.:3.9 two dishes labelled with the dye are presented. The dishes were then removed and washed in milli-Q water in order to clean off the excess of solution. Successively, the PP samples were immersed in a known volume of a $10^{-2}\,M$ solution of HCl in water/ethanol (1:1) as shown in fig.:3.10. The dye concentration was measured spectrophotometrically using a calibration curve. The density of the COOH groups

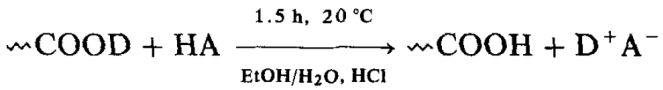

Figure 3.10: Reaction of desorption of the dye

was then calculated from the moles of thioninacetate and the volume of the coating (surface area of the PP sample multiplied for thickness of the ppAAc layer) because every Thionin Acetate (THA) molecule bonds only with one COOH group.

At this point, it is possible to measure the absorption of the solution with a spectrometer and, through a calibration curve, find the concentration of the dye and consequently, since every molecule of the dye bounds only to one carboxy group, the concentration of COOH groups. Knowing the exact volume of the solution it is a trivial matter calculating the absolute number of groups. Furthermore, we know the area of the sample and with the aim of the AFM, the thickness of the films. If now we suppose that the THA is able to rich every active group into the deposited layer, we can calculate the density of carboxy groups of the film. In Figure 3.11 the image of two disks of PP plasma treated with acrylic acid after the immersion into the thioninacetate. This technique has the advantage of a qualitative and immediate check of the quality of the treatment, it is in fact evident at a sight the uniformity and coloration of the film.

3.3.4 XPS

the working principle of the X-Ray Photoelectron Spectroscopy (XPS) technique lay in the possibility of exciting the internal shells of an atom. The spectrum emitted from the de-excitation of these excited levels returns a recognizable pattern of peaks associated to a particular chemical element. Moreover, analyzing the shifting of the measured frequency with respect to those tabulated, it is possible to study the nature of the

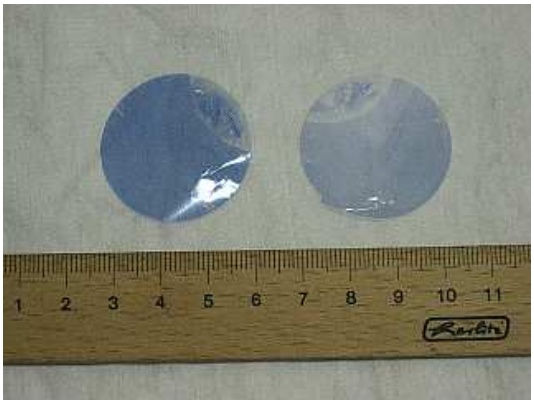

Figure 3.11: ppAAc disks after the immersion in a solution of THA

bonds in witch an element is involved. Another important characteristic is that the scanning depth of this technique is less than $10\,nm$, so a very thin layer of material can be analyzed and in our case this depth is always smaller than than the thickness of the deposited layer.

Chapter 4

Results and Analysis

4.1 Treatments

At first the rich mixture (AAc flow 9 $sccm$, Ar flow 1 $sccm$) was tested at a fixed treatment time of 20 min and at a working pressure of 10 Pa into the reactor A. Samples of polypropylene and silicon wafer were treated together in order to find out the minimum stability power and the density of carboxy group deposited. The experiments were carried out at different treatment powers, ranging from 20 W up to 120 W. After the treatment a part of the polypropylene samples were rinsed with water and Phosphate Buffer Saline (PBS) at 37°C for 24 hours for checking the stability of the deposition. Through ATR measurements, stable films were found out at a power of 100 W for the water and 110 W for the PBS.

Than a new set of measurements varying the feed composition were carried out with the equi molar mixture (AAc flow 3 $sccm$, Ar flow 3.3 $sccm$). In this case the treatment was prolonged for 30 min for increasing the thickness of the deposition for a good signal during ATR measurements. In fact, at same treatment times, thickness is directly proportional to AAc flow.

A further step was done using the last mixture, the acrylic acid poor one (AAc flow 1.25 $sccm$, Ar flow 3.3 $sccm$). This was the one with

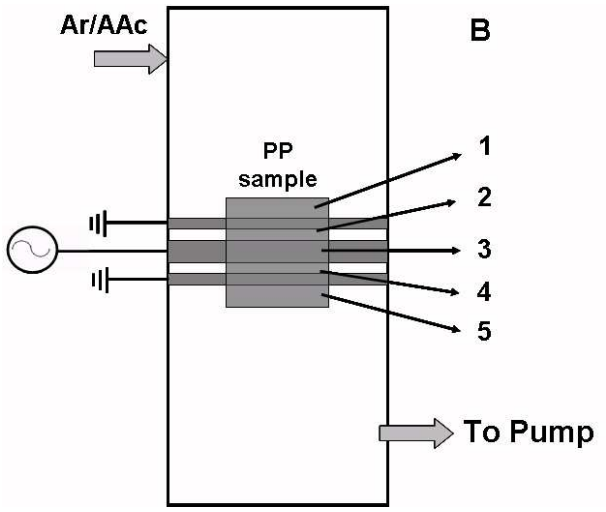

Figure 4.1: Reactor B: the positions onto the sample inside the chamber are numbered in Arabic numeral from 1 to 5. Number 1 refers to the position with the lowest resident time and 5 is the highest.

the lower achievable ratio value between the fluxes of acrylic acid and argon, with the previously described experimental apparatus. Having fixed the working pressure the only way for further reducing the ratio was diminishing the monomer flow, but it was not possible. Using an higher flow of carrier gas led to a rising in the pressure treatment and to a formation of powders.

Next, the reactor B was employed but only with the mixture poor acrylic acid mixture, that witch gave the best results on reactor A and because it revealed to produce films with the richest carboxyl groups concentration among the different stable films prepared on reactor A.

Since the specific shape of the reactor B, the monomer residence time into the plasma phase depends from the position of the sample as showed in fig. 4.1. The positions were numbered with Arabic numeral from 1 to 5 and that numbered with 1 is the nearest to the gas mixture inlet and consequently, the monomer molecules reach this site first, remaining in

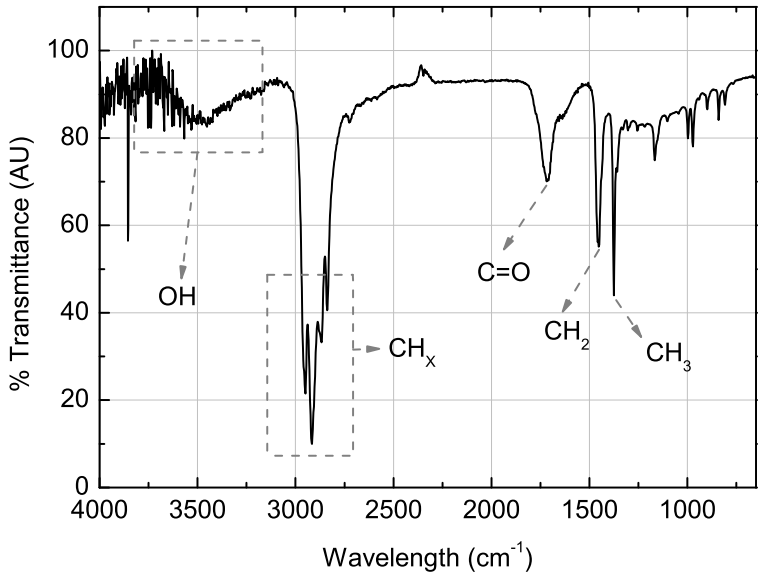

Figure 4.2: A typical ATR spectrum of a PP samples coated with polymerized acrylic acid. This spectrum refers to a sample treated for 20 min at a power 120W with the rich acid feed.

the plasma phase for a lower time than those interacting with the site numbered with 5.

Monomer residence time is an important parameter of plasma polymerization. The coating compositions and their stability were investigated for the previously numbered zones of the PP substrates in the plasma reactor.

4.2 ATR Analysis

Exploiting the fact that the ATR analysis probes the sample for a depth far greater than the film thickness, the characteristic bonds of PP, the CH_x stretching band at $3000 - 2750\,cm^{-1}$, the CH_2 bending band at $1455\,cm^{-1}$ and the CH_3 bending band at $1370\,cm^{-1}$ together with that of the ppAAc coating, the OH stretching band at $3300 - 3600\,cm^{-1}$ and

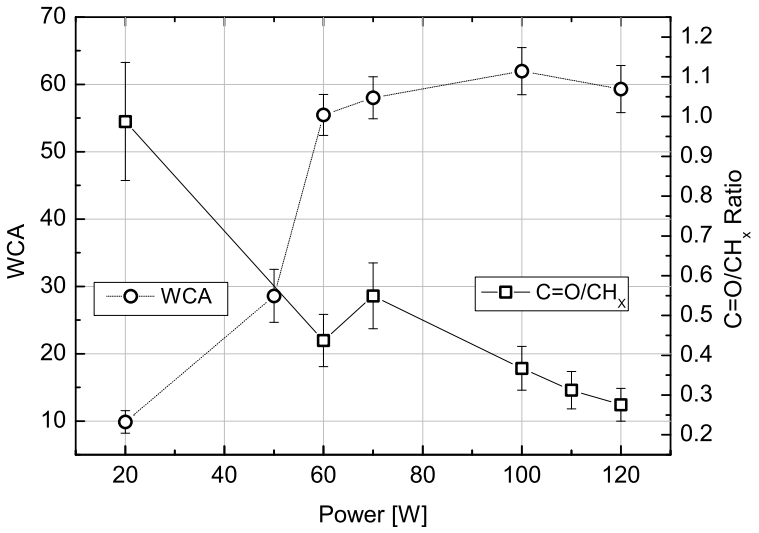

Figure 4.3: On the left: water contact angle; on the right: ratio between ATR peaks of COOH and CH_x after the washing stages. Samples of PP are treated at different power ranging from 20 to 120 W with the rich acrylic mixture for 20 min.

the C=O stretching band at 1715 cm^{-1} [26], could be detected at the same time as shown in fig. 4.2. As a measurement of the retention of the monomer structure, the ratio between C=O of ppAAc and CH_x of PP and ppAAc can be used [24]. The graph refers itself to a sample treated in the reactor A for 20 min at 120 W.

On the right side of the fig. 4.3 the ratio between the ATR peaks of COOH and CH_x is reported in function of treatment power. The value of the ratio decreases at increasing power treatment, this can be interpreted as a decreasing number of carboxylic groups onto the surface, due to the fact that higher is the power, greater is the fragmentation of the monomer. This effect is exploited for gaining in stability but it reduces the availability of groups on the surface. A compromise has to be found between stability and surface density groups.

In fact, due to the chemical conformation of the acrylic acid, it has a

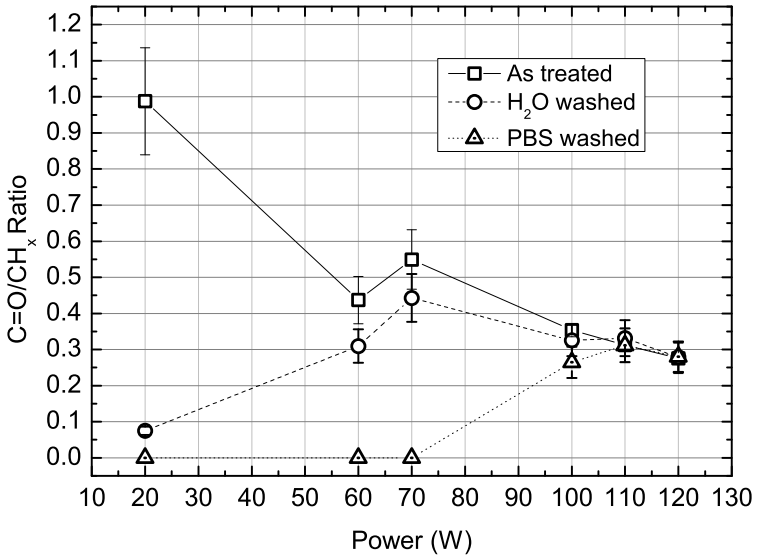

Figure 4.4: Graph showing the stability of the coating after 24H rinsing in H_2O and PBS. Samples of PP are treated at different power ranging from 20 to 120 W with the rich acrylic mixture for 20 min.

double bond between two of its backbone carbon atoms. The opening of this bond leaves two free electrons ready to form new bonds leading to the polymerization process. What happens is the formation of a linear polymer. If all the polymerization process would lead to linear chains, what one has would be something like a "spaghetti-like" ensemble deposited onto the PP substrate, with some bond on the substrate. Putting such a sample in a water solution would lead to an easy dissolution of those "spaghetti" into the water.

Increasing the discharge power allows to open other bonds of the acid that permit to form more than two bonds per molecule, giving rise to a crosslink, leading to a deposition more similar to a net. Obviously, this shape gives more stability to the deposition but, because of this operation is not selective, many carboxyl groups are missing despite stability.

On the left side of the same figure 4.3, the static water CA are re-

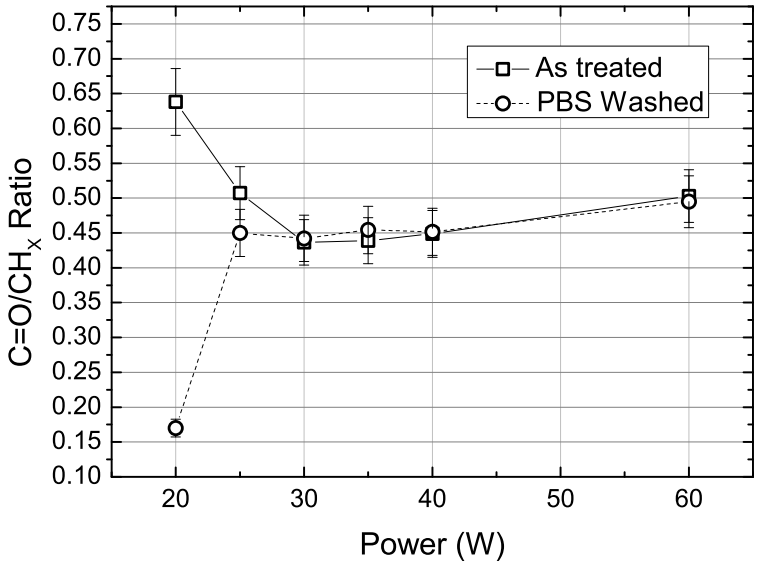

Figure 4.5: Ratio between C=O an CH_x bands of PP and pp-AAc after the washing in PBS. This sample was treated for $30\,min$ at different power ranging from $20\,W$ to $60\,W$ with the poor acrylic mixture into the reactor A.

ported. These values are increasing with the power and at the light of the fact that carboxy groups have an hydrophilic character, more they are, lower is the angle. This confirms and enforces the former hypotheses about the number of groups on the surface.

Another figure (4.4) shows the ratio of ATR peaks of C=O and CH_x before and after the washing stage of the same sample, revealing the power at which the coatings have to be considered stable. As we can see in this figure 4.4, the curve of the water washed sample is superimposed to the unwashed one for a power of $100\,W$ and $110\,W$ for the PBS washed sample.

New set of measurements were carried out with the other two mixtures. A plot (fig.4.5) representing, as for the previous feed composition, the ratio between COOH and CH_x peaks after PBS washing in function of treatment power for the poor mixture, shows that $30\,W$ is the mini-

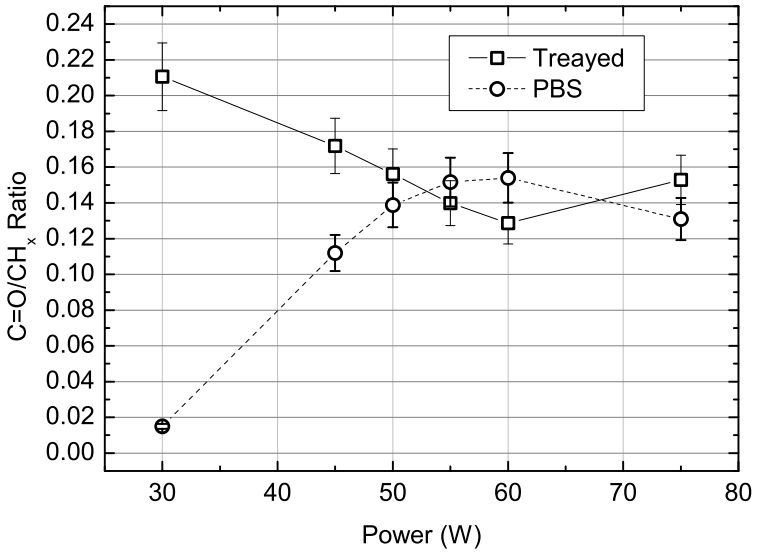

Figure 4.6: Ratio between C=O an CH_x bands of PP and pp-AAc after the washing in PBS. This samples were treated for $20\,min$ at different power ranging from $30\,W$ to $75\,W$ with the equi molar acrylic mixture into the reactor A.

mum stability power for this feed. At the end, the last feed composition, the equi molar acrylic acid mixture, presents a graph with the same characteristics of the previous and the minimum stability power riches $50\,W$ (fig.4.6).

Looking at the graphs in fig. 4.5 and 4.4, we notice that the retention of the monomer structure decreases at increasing input power. This behaviour can be explained as an increased fragmentation of the monomer with the power. This fragmentation enhances the crosslinking ability of the plasma polymer to form a more stable coating.

For a quantitative evaluation of the inserted groups, an accurate analysis of the number of carboxy groups was done labelling four different treated samples for every different treatment power, with dyes.

Also reactor B was employed but only with the poor mixture, be-

cause it was the best condition in reactor A. Fig. 4.7 reports C=O/CH_x band ratios measured on plasma coated PP substrates before and after washing in PBS at the five different positions as pictured in fig.4.1. Deposition was performed at $10\,W$, the minimum power input at which the coating was stable in almost all the investigated positions (partially stable in the position 2, totally stable in 3, 4 and 5). This power input value is considerable lower ($\sim 1/3$) than that obtained with the same feed composition on the reactor A. The reason lies in the fact that the discharge volume of the reactor B is lower with respect to the reactor A. The relation between the two discharge volume is: $V_A \approx 2.5 \cdot V_B$ where V_A and V_B are the discharge volumes respectively. Because the power is mainly consumed inside the electrodes, this well correlates with the different power inputs ($30\,W$ in reactor A against $10\,W$ in B).

At lower power input the stability in PBS of the ppAAc decreases.

By observing fig. 4.7 it is possible to note another important characteristic deriving from the geometry of the plasma reactor. Stability of the coatings increases going from the position 1 to the position 5 of the substrate in the plasma reactor. Kelly [27] experimentally demonstrated (using a plasma reactor similar to the reactor B) that the chemical composition of ppAAc (in particular the COOH groups retention) is influenced by the residence time of the monomer in the plasma phase, as a consequence of the increased monomer fragmentation. This work shows for the first time that not only the chemical composition of the ppAAc layers is influenced by the substrate position but their stability in aqueous solutions too. The two phenomena are correlated, since both can be charged to the increased monomer fragmentation that leads to higher cross-linked and lesser hydrophilic and functionalized coatings.

Fig. 4.7 also shows a particular trend for the C=O/CH_x ratio measured at the different substrate positions. However, since the deposition rates were different in function of the position, the trend could be influenced by the different coating thicknesses. For this reason a better

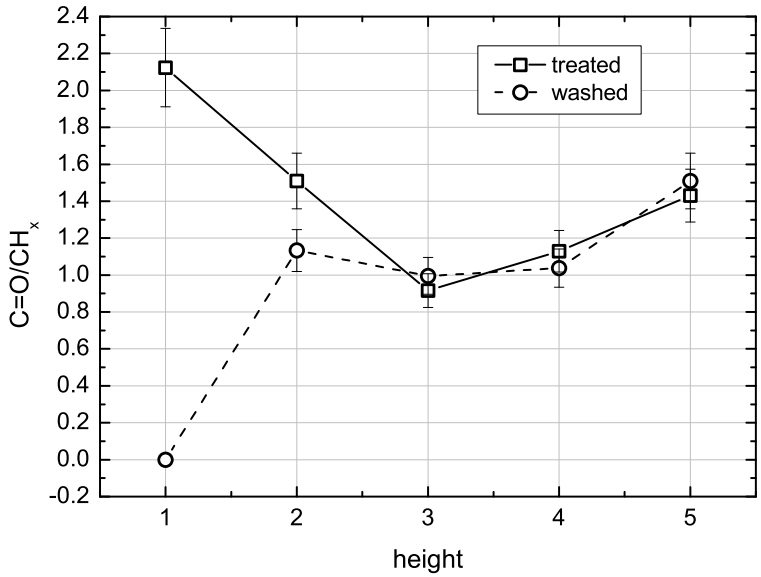

Figure 4.7: Ratio between C=O and CH_x bands of the sample treated at $10\,W$ into the reactor B, in the five different positions described in figure 4.1

evaluation of the COOH concentration of the coatings was performed by reaction with thioninacetate.

4.3 AFM Analysis

Analysis of the substrates with the aim of the AFM showed the morphology of the coatings. The figures 4.8, 4.9 and 4.10 show three samples of PP treated at three different Radio Frequency (RF) power input but with the same feed composition, the AAc rich one, after water washing stage.

The upper left image presents the coating obtained ad $20\,W$ input power, almost totally delaminated. In the upper right, the sample prepared at $60\,W$ input power, the holes are smaller but already present together with many cracks. The sample obtained at $100\,W$ input power, positioned bottom left, it is smooth without holes or cracks and corre-

Power (W)	Flux ($sccm$)	Growing rate (nm/min)
30	AAc poor	4.4
50	AAc equi	6.7
110	AAc rich	10

Table 4.1: Growing rate of different power treatment and feed composition into the reactor A

spond to the stable coating.

4.3.1 Film growing rate

With the aim of the AFM, set of measurements were carried out for measuring the thickness of each sample and evaluating the growing rate of the films. Plotting the thickness in function of treatment time shows a linear trend which slope is the growing rate. In tab. 4.1 the data of the growing rates of films in the reactor A are presented. It is evident that the deposition rate is greater for higher monomer fluxes, as expected. Furthermore, the intercept of the curve fitting the data does not cross the origin of the coordinate axis, instead its value is negative. This can be explained as an effect of the etching process during the activation stage, where RF was acting only at the presence of argon gas, namely without deposition, and in the first instances of the deposition process before the equilibrium conditions were reached. No supplementary trials were performed in order to better understand and quantify the phenomenon.

4.4 Active groups concentration by thioninacetate labelling

Figure 4.11 reports the density of the active sites of samples treated into the reactor A at $30\,W$ with poor acrylic mixture for five values of

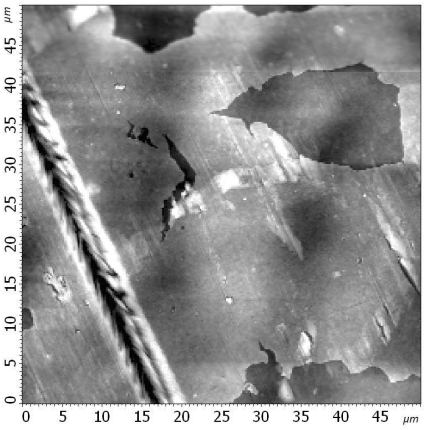

Figure 4.8: $20\,W$ water washed

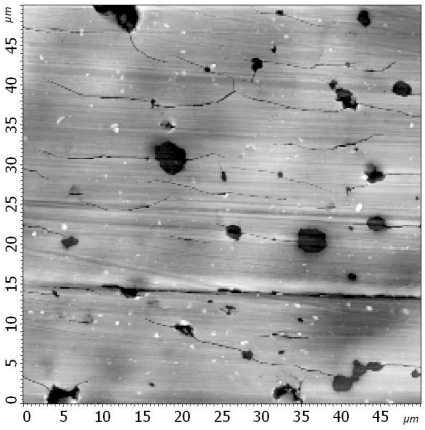

Figure 4.9: $60\,W$ water washed

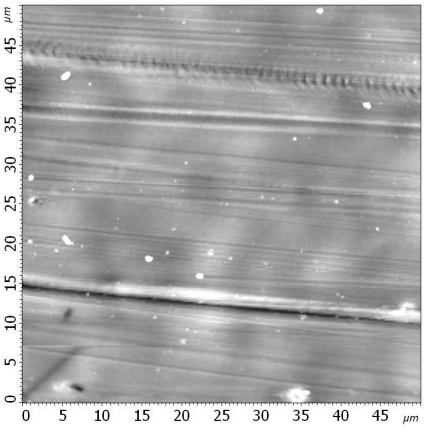

Figure 4.10: $100\,W$ water washed

Square images of $50 \times 50\ \mu m$ of the ppAAc films washed in water after a deposition at $20\,W$, $60\,W$ and $100\,W$ RF input power into the reactor A, respectively.

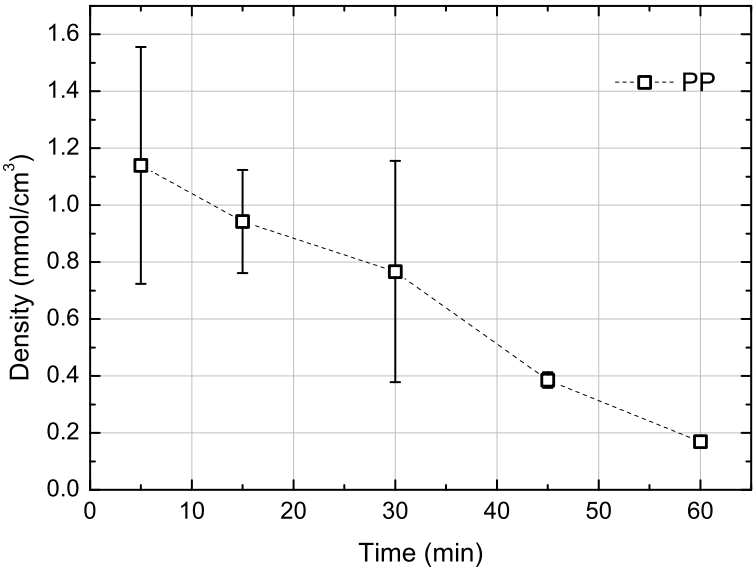

Figure 4.11: Concentration of active sites in function of the film thickness obtained with a treatment into reactor A at $30\,W$ with the poor acrylic acid mixture.

treatment time ranging from 5 to $60\,min$. This number increases while the time is decreasing although it was expected to be constant. The first hypothesis is that not all the groups are reached from the dye, and that it depends from how deep each group is buried. In fact, longer is the treatment thicker is the deposition. Against this supposition, Ivanov [28] reported that this dye penetrates easily into a ppAAc coating, at least $150\,nm$ in 10 hours.

As a second hypothesis, it is possible that the vacuum radiations and plasma species bombarding the coating had been spoiling the material, not only on the surface but more deeply too. This will be discussed later in chapter 5.

For these reasons, as a measurements of the superficial density of groups, it is better taking the value at the thinest thickness obtained among all treatments of a specific set of parameters, namely, using the

Reactor	Volume density $mmol/cm^3$	Surface density $mmol/cm^2$	Author
A	$\rho = 1.1$	$\sigma = 1.4 \cdot 10^{-6}$	This work[29]
B	$\rho = 1.8$	$\sigma = 4.6 \cdot 10^{-6}$	This work[29]
-	-	$\sigma = 2.3 \cdot 10^{-6}$	Detomaso[30]
-	$\rho = 1.7$	-	Sciarratta[31]

Table 4.2: Concentration of COOH groups from the results of this thesis work in comparison to some literature data.

sample treated with a specific gas feed and power but with the minimum treatment time. The thinest thickness obtained was of $10\,nm$ corresponding to a treatment time of $5\,min$ into the reactor A with the poor feed at $30\,W$.

Although the higher value for surface density is $4.6 \cdot 10^{-6}\,mmol/cm^2$ obtained on reactor B, it is better, for the previous construction, using the value from reactor A. The best value for surface density on reactor A is $1.4 \cdot 10^{-6}\,mmol/cm^2$, calculated considering all the active groups onto the surface.

The best value for the volume density is around $1.8\,mmol/cm^3$ and was reached on reactor B. All these values can be compared to the recent literature data reported in table 4.2.

The renormalization of the energy per unit volume, due to the different volume of the two reactors is in agreement with the stability power, it means that at equal input power and feed composition the power per monomer unit has to be the same and the only difference has to be seek in the different reactor configuration. In case of reactor A, the monomer is forced passing through the showered antenna, the zone where the energy is the greatest, that is not true for the case of reactor B. This could be the reason that leads to an higher density of COOH groups generated in reactor B with respect to the reactor A.

Fig. 4.12 shows the COOH groups concentration for different substrates positions and deposition times of a sample treated in the reactor B at $10\,W$ for $10\,mim$. No clear trends are observed by varying the deposition times, although for position 4 a slight increase of the COOH concentration was detected. For other positions, the concentration was almost constant, differently from what observed on reactor A.

The biggest differences come from the different positions. The trend is in agreement with the $C{=}O/CH_x$ ratio measured on ATR spectra, showing a minimum in carboxy groups retention on position 3, corresponding at the position of the antenna, and a maximum in position 2, corresponding to the lowest resident time. Moreover, because COOH concentration increases in position 4 respect to the position 3, the minimum in carboxy acid concentration can be supposed deriving not only from higher monomer fragmentation but also to an additional damaging due to stronger plasma species bombardment on the growing ppAAc layer.

Also the samples treated with the other feed composition were labelled with the dye. The equi-molar feed treated substrate gave values inferior to those obtained respect with the poor feed ones. The rich feed, instead, was so poor of groups that this method was not able to measure the retention of carboxylic groups.

An explanation is given by the fact that increasing the number of monomer molecules into the reactor, the energy per unit monomer is decreased and a less crosslinked deposition is formed. The increasing of the treatment power restores the good value but increases also the ions bombardment and the vacuum ultra violet radiation giving rise to an enhancing in the etching process that lowers the deposited groups.

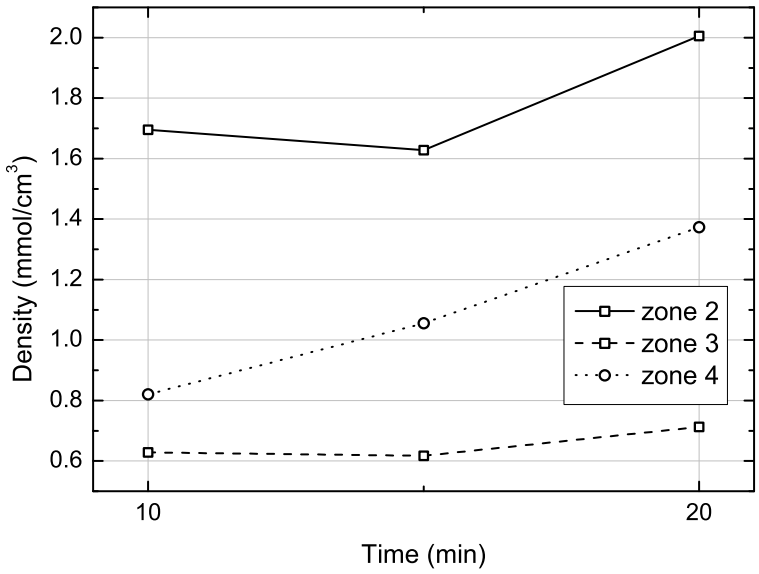

Figure 4.12: Density of groups at different treatment time in different zones of the sample. Only the zone numbered with 2, 3 and 4 were kept in consideration

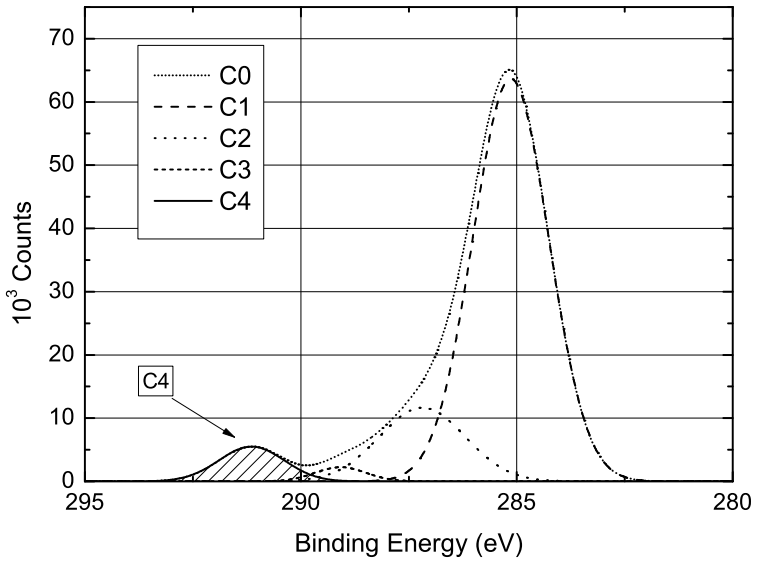

Figure 4.13: high resolution XPS spectra of C1s peak. In particular: the C4 peak of COOH/R component of the analyzed sample.

4.5 XPS Analysis

Carboxy groups concentration was evaluated by XPS analysis. Fig. 4.13 shows the XPS C1s spectra of a ppAAc layer on PP. The coating was obtained with the AAc poor mixture at the minimum power for stability ($30\,W$) in the reactor A. Since plasma polymerization was prolonged for 30 minutes, the coating thickness ($80\,nm$, as measured by AFM analysis) was far greater than the penetration depth of XPS analysis.

The spectrum can be fitted with four peaks corresponding to CH_x groups ($285.14\,eV$) labelled with $C1$, C−O groups $287.19\,eV$ labelled with $C2$, C=O and O−C−O ($289.08\,eV$) labelled with $C3$ and O−C=O groups ($291.14\,eV$) with $C4$ [32]. The $C0$ curve depicts the unfitted signal, namely the sum of the areas of the four peaks from $C1$ to $C4$.

The presence of C−O and C=O groups derives from different fragmentation and rearrangement processes that occur in the plasma phase. In a pure ester coating, C−O and O−C=O components would be expected having equal intensity. In the spectrum of fig. 4.13, the C−O component is greater than the O−C=O one, as a consequence of the high fragmentation conditions required to obtain stable coatings.

It is well known that the carboxy group in ppAAc is present both as carboxy acid and esters and that the extent of COOH insertion strongly depends on plasma deposition parameters. Carboxy acid groups can be easily distinguished from esters by chemical derivatization (for instance with trifluoro ethanol) followed by XPS analysis. However, no derivatization was performed in this work to distinguish the acid (COOH) and the ester (COOR) contributions to the O−C=O component, but acid groups concentration has been carefully evaluated with dye assay.

Table 4.3 shows the O/C ratio and the COOH/R groups component (from C1s peak deconvolution) of differently prepared samples. The ppAAc coating obtained with the poor acid feed shows higher O/C ratio with respect to the ppAAc coating obtained from the rich mixture. The O/C ratio measured on stable coatings well correlates with their

Reactor	XPS O/C %	XPS COOH/R %	Author
A_{rich}	21	2.9	This work[29]
A_{poor}	33	5.7	This work[29]
B	31	3.6	This work[29]
-	30	4	Detomaso [30]
-	-	5.2	Sciaratta [31]
-	-	<6	Alexander [25]
-	-	7	Jafari [33]

Table 4.3: Data of retention of carboxy groups in percent from C1s peaks deconvolution compared to other works

hydrophilic properties.

All the values for reactor B comes from zone 2 of the samples, the zone where the treatments had the best outcome. The table 4.2 reports a volume concentration value of COOH groups on samples prepared on reactor B, that is 60 % higher than that measured on reactor A with the same gas composition. This result does not correlate with COOH/R component of the C1s peak measured on the same samples but in different reactors, indicating predominance of esters species on ppAAc on reactor A. The higher number of COOH groups onto the samples prepared in the reactor B with respect to the reactor A derives probably from the lower residence time of the monomer in the plasma phase. In fact, by increasing the residence time in reactor B, the COOH concentration decreases below that measured on reactor A. In fact it is sufficent to look at the data relative to the position numbered with four in fig.:4.12 where the volume concentration is $0.6\,mmol/cm^3$ around one half of that treated in reactor A with the same feed composition.

Regarding the relevance of short residence times, it has to be underlined that the use of particular expedients (with the acrylic acid monomer that reach the substrate surface without passing through the plasma

Power (W)	W/FM
30	0.33
50	0.23
110	0.17

Table 4.4: Values of the scalability factor W/FM versus minimum stability power of the coatings at the three different feed composition.

zone) allows to prepare stable ppAAc layers with COOH groups concentration considerably higher than those here measured [32].

Poly(Acrylic Acid) (PAA) should have an O/C ratio equal to 67%. However, the values measured on our stable ppAAc are comparable to those available in literature and indicate a loss of monomer structure due to strong fragmentation in the plasma phase [30, 31, 25].

According with literature data (table 4.3), the COOH/R component measured on stable layers ($3\% - 6\%$) is considerably lower than that of pure poly(acrylic acid) (33%). The reason of this phenomenon lies in the necessity of employing high fragmentation conditions in order to obtain high cross-linked, stable films.

4.6 Effects of carrier gas

It is well known that plasma polymerization is a radical promoted process ruled by the composite parameter power input (W) per monomer flow (F) and molar mass of the monomer (M), $\frac{W}{FM}$ [10]. Increasing the flow makes the minimum power stability lower as stated by the measurements. It is expected that for obtaining a film with the same characteristics, this parameter (scalability factor) has to be constant but the table 4.4 shows that it is not true.

An explanation is given by Hegemann [34, 35] which supposed that an influence upon the non polymerizable gas has to be taken into account.

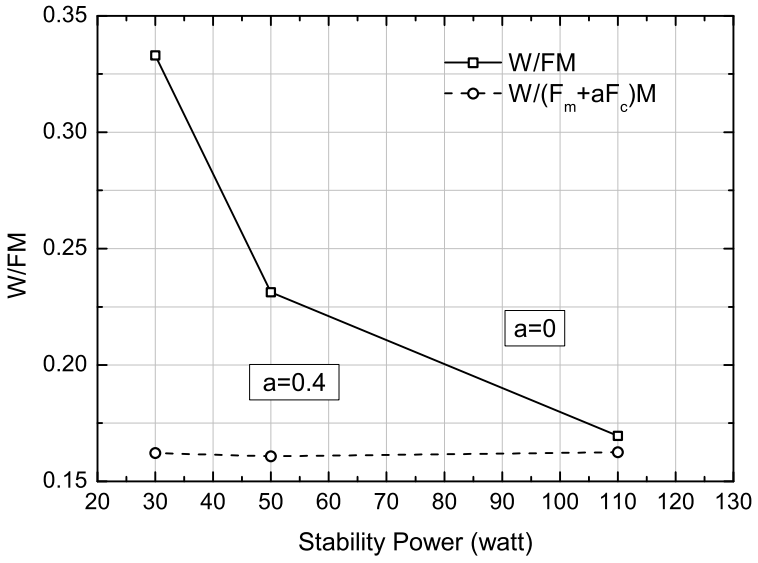

Figure 4.14: The two curves in the graph represent the scalability factor for two different value of parameter a. When a equals 0.4 the data lies on a constant line.

He inferred to think to the parameter F like a composite parameter that include the monomer flow and the carrier gas flow. He wrote $F = F_m + a \cdot F_c$, where F_m is the monomer flow, F_c the carrier gas flow and a a constant dependent from the gas and monomer kind.

In fig. 4.14 a graph showing the scalability factor plotted in function of power treatment for two different values of the parameter a is presented. When the parameter a equals 0.4 the values of the composite parameter W/FM can be considered constant. The explanation given by Hegemann was that a part of the input energy is consumed by the gas carrier and consequently that the gas flow has to be taken into account together with the monomer flow. The data refer to samples treated into the reactor A only.

Chapter 5

Vacuum Ultra Violet radiation effects upon depositions

5.1 The experimental evidence

In fig. 5.1 the total number of active groups per volumes with the same surface area are reported against film thickness. It is evident how their number is not increasing linearly with the thickness as was expected if only the deposition process and superficial etching process were acting. Starting from that experimental evidence, a simple model explaining the data trend is presented.

It has to be supposed that something acting during the treatment was removing carboxylic groups, and that it was acting allover the thickness of the film. In fact a simple etching process, that removes material only from the surface cannot explain why the total number of deposited active groups is diminishing. Some effects is accountable of the diminishing number of groups in the deeper layers of the deposition. Otherwise, a linear trend would be expected.

On the contrary, supposing a volume effect could explain the fact.

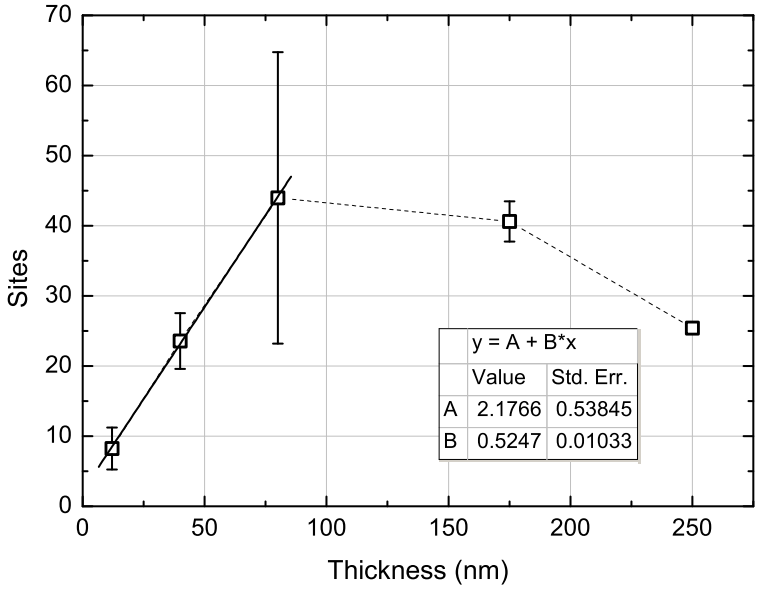

Figure 5.1: Total number of active sites per volume on a surface of $1\,nm^2$ versus films thickness. These samples were treated in the reactor A at 30 W.

Let suppose an effect acting for the entire deposition process on the entire volume of the deposition, the layers that are first deposited, those which will be buried below other layers and will become the deepest, will undergo the effect for a longer time with respect to the latest deposited ones. Namely, the external layers of the coating has to retain a grater number of groups respect to deeper layers. Obviously, at the same time the deposition and the etching effects are acting too.

5.2 The model

Let supposed that the number of deposited groups depended from three main factors: the deposition, the etching and a VUV radiation generated form the glow discharge [36, 37].

The process can be seen as a sequence of following instants, during which the total amount of deposited material, N_i, is the sum of the three effects.

$$N_{i+1} = (N_i + a)b \tag{5.1}$$

where a takes in account the effect of deposition and etching, supposed constant for the entire process and b the VUV effects.

Let N_0 the initial number of sites, then:

$$N_1 = (N_0 + a)b$$
$$N_2 = (N_1 + a)b = ((N_0 + a)b + a)b = (N_0 + a)b^2 + ab$$
$$N_3 = \cdots = (N_0 + a)b^3 + ab^2 + ab$$
$$\cdots\cdots$$
$$\cdots\cdots$$
$$N_n = (N_0 + a)b^n + a\sum_{i=1}^{n-1} b^n$$

if $N_0 = 0$ typical before deposition

$$N_n = a\sum_{i=1}^{n} b^i \tag{5.2}$$

because the contribution of b is: decreasing the multiplied factor every step, it has to be less than 1, hence:

$$\lim_{n\to\infty} a\sum_{i=1}^{i=n} b^i = a\left(\frac{1}{1-b} - 1\right) = \frac{ab}{1-b} \tag{5.3}$$

$$\text{since that: } \lim_{n\to\infty} N_n = \frac{ab}{1-b} \tag{5.4}$$

Following the theory, the number of total sites could reach the constant value $ab/(1-b)$, but looking at the graph in fig. 5.1 reveals that it is not true. In fact the total number of groups is decreasing after a certain amount of time.

At this point a further observation can be done, during the treatment, the total pressure in the reactor was slightly slowing down.

In fig: 5.2 the trend of the pressure during the treatment shows a decrease of about 1 Pa in 20 min with an exponential decay. During the treatment the monomer is evaporating into the acid flask while its vapours are flowing trough the needle valve into the reactor. The evaporation of AAc consumes energy in form of latent heat of evaporation,

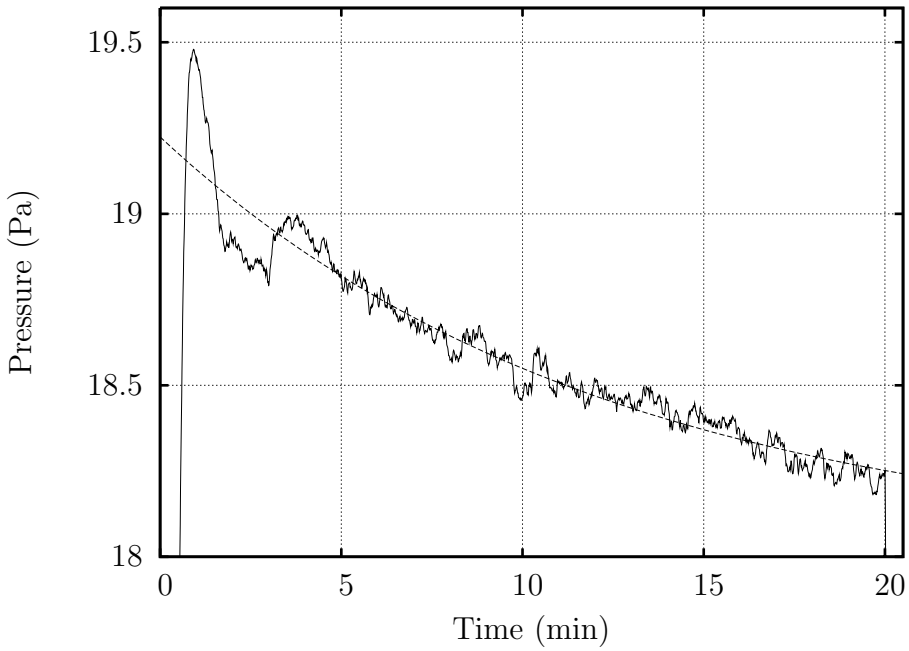

Figure 5.2: Treatment pressure in function of treatment time in reactor A

this loss of energy causes a decrease of the temperature of the acid in the flask, that causes a decrease of the vapour pressure of the acid and a consequent decrease of its flow.

So, a new parameter has to be entered in the formula 5.5. The task of this parameter is lowering, step by step, the number of incoming monomer molecules towards the sample. This quantity influences the parameter a like a multiplying factor c with a value inferior to the unity.

What we have now is a system of two expression:

$$\begin{cases} N_{i+1} = (N_i + a_i)b \\ a_{i+1} = a_i c \end{cases} \tag{5.5}$$

as in the former case N_0 the initial number of active sites on the surface and a_0 the parameter when pressure effect is not jet acting, reiterating

we have:

$$\begin{cases} N_1 = (N_0 + a_0)b \\ a_1 = a_0 c \end{cases}$$

$$\begin{cases} N_2 = ((N_0 + a_0)b + a_1)b = (N_0 + a_0)b^2 + a_0 c \\ a_2 = a_1 c = a_0 c^2 \end{cases}$$

$$N_3 = \cdots = (N_0 + a_0)b^3 + a_0 c b^2 + a_0 c^2 b$$

$\cdots\cdots$

$\cdots\cdots$

$$N_n = (N_0 + a_0)b^n + a_0 c b^{n-1} + a_0 c^2 b^{n-2} + \cdots + a_0 c^{n-1} b$$

if $N_0 = 0$:

$$N_n = a_0 b^n + a_0 c b^{n-1} + a_0 c^2 b^{n-2} + \cdots + a_0 c^{n-1} b \tag{5.6}$$

$$N_n = a_0 b^n + a_0 \sum_{i=1}^{n-1} b^i c^{n-i} = a_0 b^n + a_0 \sum_{i=1}^{n-1} b^{n-i} c^i$$

$$N_n = a_0 b^n + a_0 b^n \sum_{i=1}^{n-1} \left(\frac{c}{b}\right)^i = a_0 b^n + a_0 c^n \sum_{i=1}^{n-1} \left(\frac{b}{c}\right)^i \tag{5.7}$$

where N_n is the total number of active groups present into the whole deposited film at the nth step. Going forward with the same method previously used, it is possible to foresee the behaviour of this succession at a very long time, namely for $n \to \infty$.

The first term of the succession 5.7 cancels out for $n \to \infty$. The second term

$$\lim_{n\to\infty} \sum_{i=1}^{n-1} \left(\frac{c}{b}\right)^i \overset{c<b}{=} \frac{1}{1 - \left(\frac{c}{b}\right)} - 1 = \frac{c}{b - c} \tag{5.8}$$

$$\lim_{n\to\infty} \sum_{i=1}^{n-1} \left(\frac{b}{c}\right)^i \overset{b<c}{=} \frac{1}{1 - \left(\frac{b}{c}\right)} - 1 = \frac{b}{c - b} \tag{5.9}$$

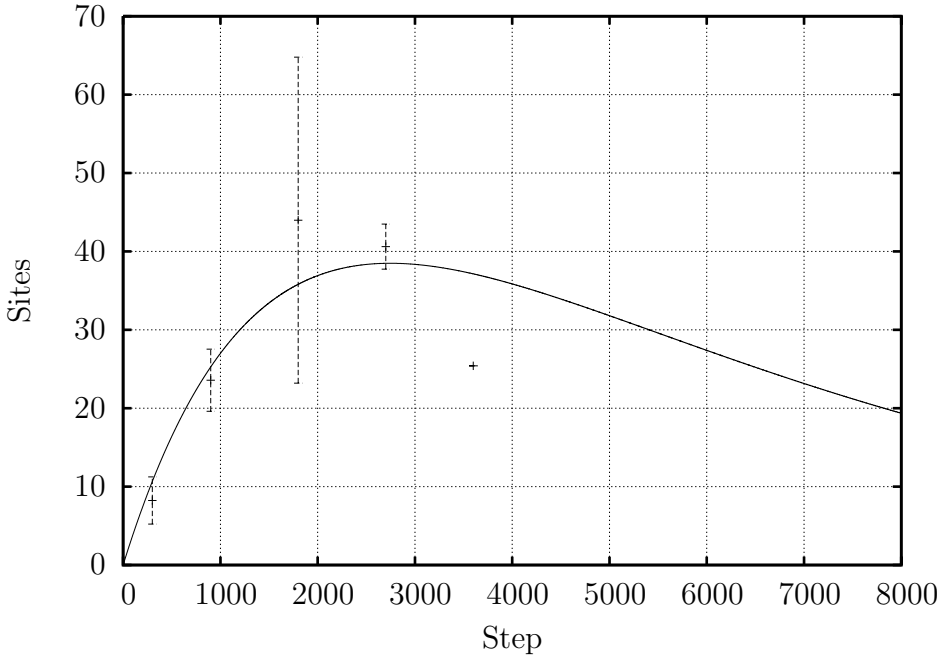

Figure 5.3: The continuous line represents the simulated data while the points with the error bars are the measured data

and at the end:

$$N_n \overset{c<b}{=} a_0 b^n + \frac{a_0 b^n c}{b-c} \underset{n\to\infty}{\longrightarrow} 0 \tag{5.10}$$

$$N_n \overset{b<c}{=} a_0 b^n + \frac{a_0 c^n b}{c-b} \underset{n\to\infty}{\longrightarrow} 0 \tag{5.11}$$

The expression in 5.10 holds only for $c < b$ and 5.11 for $b < c$. Patameters b and c are interchangeable and their exchange does not influence the result.

However, with the aim of a computer, it is easy to simulate the evolution of the total number N_n of sites, step by step, finding a curve to use for comparing real data. In appendix B the code of the program.

Chapter 6

PEG grafting and applications

6.1 Protein adsorption

When a solid surface is exposed to an aqueous protein solution, typically accumulation of protein molecules at the solid/liquid interface occurs. The interaction of proteins with material surfaces plays a key role in a variety of fields, including biotechnology and biomaterial science. In this sense, controlling cell-material interactions is of crucial importance for the development of new biomaterials and biosensors. It is a general trend to try to relate the characteristics of the adsorbed protein layer and the cell behavior to the wettability of the material surface. However, several driving forces determine the protein adsorption process, including redistribution of charged groups in the interfacial film, dehydration of protein and substratum surface and structural rearrangement in the protein molecules. Concerning the substrate characteristics, both surface chemistry and topography affect protein adsorption and cell adhesion [38].

In fig. 6.1 the protein fluorescence intensity is reported for tree samples of PP, the non treated sample taken as reference, a sample treated

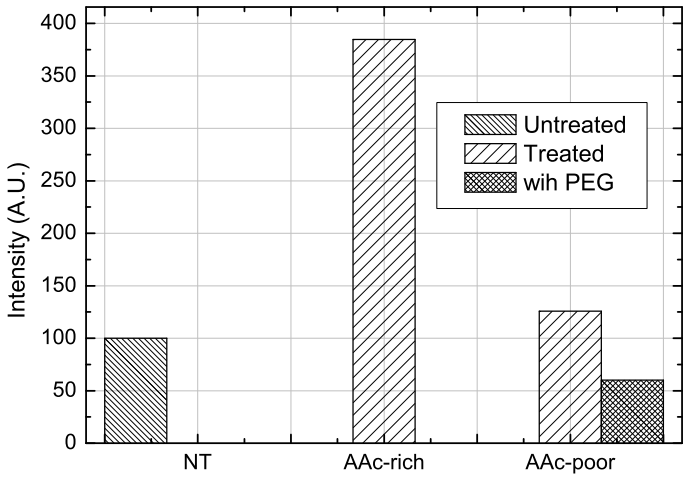

Figure 6.1: Normalized protein fluorescence intensity respect to the Non Treated (NT) PP substrate

as described in previous chapter with the acrylic acid rich mixture and the last, the one treated with the acrylic acid poor mixture. For the case of last sample, PEG chains were attached to the COOH groups available onto the surface.

This result contrast with the general trend to try to correlate protein adsorption to wettability of the surface. In fact ppAAc surfaces show higher wettability (contact angle 60°) than PP ones (contact angle 103°). Generally, hydrophobic interactions are indicated as the main driving forces determining protein adsorption. However, this results strongly indicates that wettability of the surface cannot determine alone the overall protein adsorption process. This results seem to contrast with other literature data concerning protein adsorption on plasma polymerized acryl acid coatings. In those cases, the carboxylic-containing coatings were found to inhibit protein adsorption, probably due to electrostatic repulsion between such surfaces and proteins, which are both negatively

charged at neutral pH. In our case, instead, the sample treated with the rich mixture seems to increase the protein adsorption but here we have very low concentration of carboxy groups. In these conditions, electrostatic repulsion effects could be negligible and the prepared surface results optimal for protein adsorption. Increasing the number of active groups on the surface leads to a opposite situation in which the adsorption is diminished. Moreover, the sample with PEG shows a smaller adsorption due to the PEG properties.

This facts underlines how the functionalization of PP through the previously described treatments can be useful for the production of biomaterials.

A detailed explanation on how the PEG chains are attached to COOH functionalized coating can be found in appendix C.

6.2 Covalent biofunctionalisation of hydroxyapatite scaffolds via plasma technology

The knowledge of articular cartilage, calcified cartilage and bone tissue architectures as well as the biological mechanisms involved in the maintenance of their structure and function is essential for the design of new biomaterial scaffolds (fig. 6.2) with properties such as tissue compatibility, regeneration induction and growth that could potentially enhance innate restorative capacity. It has been widely described the ability of bioceramics such as hydroxyapatite (HA) and bioactive glass ceramics to form a bonding with the surrounding bone tissue. However, these materials alone do not match the specific requirements of bone tissue and specially the calcified cartilage interface. For this reason, researchers try to combine these inorganic materials with organic matrices that can improve cell-biomaterial scaffold interactions thereby enhancing new tissue growth. In addition, stable linking of ligands to a surface is essential to promote cell interactions with the surface of biomaterials, in order to avoid the redistribution of weakly adsorbed ligands. Derivatization of bioceramics for ligand introduction ideally should allow covalent linkage to the inorganic matrices e.g. via functional groups like hydroxyl-,

Figure 6.2: Image of HA scaffolds

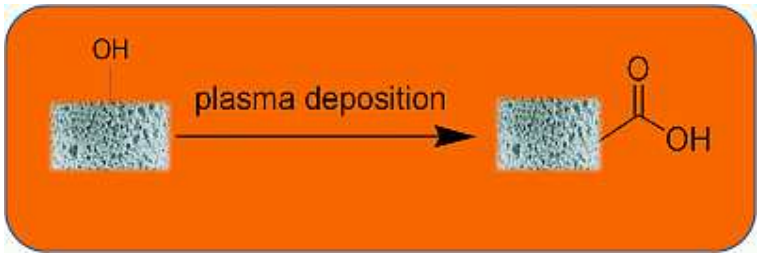

Figure 6.3: The insertion oh carboxy groups on the surface of the scaffolds

amino-, or carboxyl groups. A possibility to introduce modifiable groups on the hydroxyapatite scaffold is plasma deposition (fig. 6.3).

Stable ppAAc coatings were plasma deposited onto porous HA scaffolds ($5 \times 5 \times 5\,mm^3$) [39]. Depositions were performed in the previuosly descrubed reactor A with the poor acrylic acide mixture,(1.25 $sccm$ acrylic acid, 3.3 $sccm$ Ar). Depositions were performed at a power input of 30 W and with a duration of 30 min. Stability of the plasma deposit was assessed by immersion in PBS for 20 hours at 37°C.

6.3 Thickness of a grafted layer of PEG onto a ppAAc film: measure and Monte Carlo simulation

In this work the deposition of linear polymers such as polyethylene glycol on a plasma treated surfece has been studied experimentally and theoretically by means of a Monte Carlo simulation. In particular the substrate utilized for that work were functionalized with the methods previously described in this thesis.

Pieces of $1\,cm^2$ of silicon wafer has been located inside the cylindrical stainless steel vacuum chamber described as reactor A. The plasma treatment was performed at $30\,W$ with the poor acrylic mixture. The treated samples were grafted with PEG following the procedure described in appendix C and chains of two different length were attached (3000 and 5000 Dalton). At the and the AFM were used to measure the thickness of the grafted samples. The thickness difference between the grafted side of the sample with respect the non grafted side gave the effective PEG thickness layer.

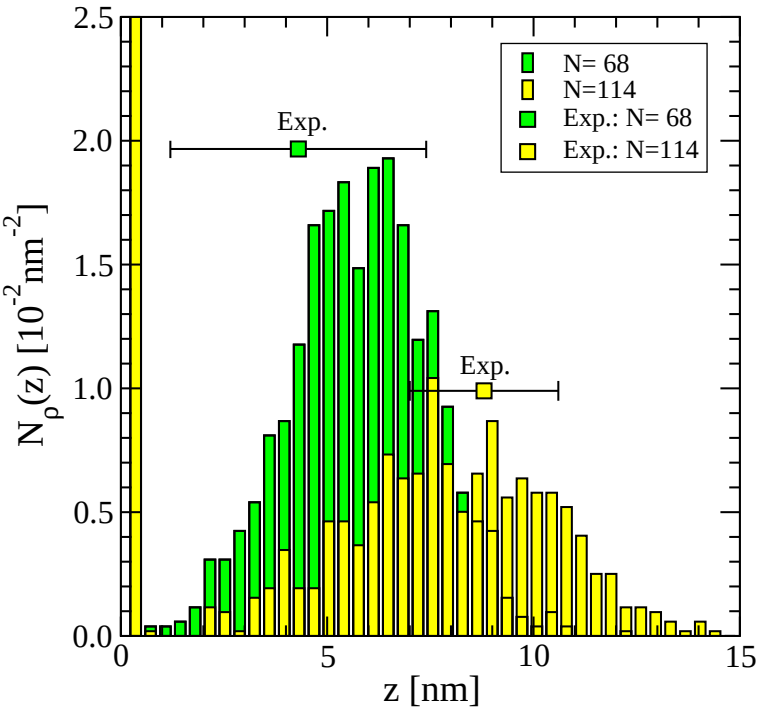

Figure 6.4: Heights of PEG layer from simulation and direct measurement by AFM.

Chapter 7

Conclusion

In this thesis a plasma process for deposition of thin films of poly acrylic acid onto polypropylene substrate were performed and optimized for two different reactors. The first reactor is a capacitively coupled parallel plate reactor with a antenna shaped as a shower where the precursor is forced to pass through the holes of the antenna. The second reactor was realized to avoid the monomers of the acid passing through the antenna and the consequent spoiling of the monomers themselves. This expedient allowed to deposits with a greater number of carboxylic groups onto the surface.

The deposited thin films were characterized with a complete set of measures and instruments from which the thickness, density of active groups and composition were collected. The properties of the treated samples were tested through interaction with fibrinogen proteins and with Poly Ethylene Glicole chains.

The work so far done has been utilised in a new application for creating a functionalized layer between hydroxyapatite and bone tissues. Here the researchers wanted to make the hydroxyapatite biocompatible, exactly what this work was intended to.

Moreover, a model concerning the total number of deposited groups into the whole deposition layer, was done. The idea of this model was born from the observation that the total number of deposited groups in

function of thickness or deposition time in not a linear function. This fact can be explained considering a volume effect of the Vacuum Ultra Violet radiation generated from the glow discharge.

The prediction of the model are in good agreement with the collected data.

The interest for plasma treatment is biocompatibility is already high as the big number of recent published articles attests. This work gave a contribution to the complex argument of plasma polymerization presenting, for the first time, stability test in phosphate buffer saline solution. It could be a minor improvement but it has to keep in mind that quite all biocompatibility test has to be done in a physiological solution, that is, a saline solution.

Appendix A

The radiometer of Croockes

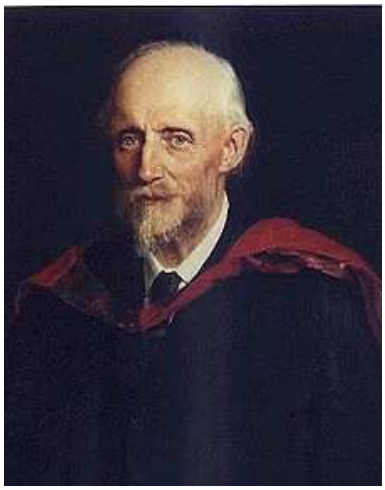

Figure A.1: Osbourne Reynolds (1842-1912)

Reynolds found that if a porous plate is kept hotter on one side than the other, the interactions between gas molecules and the plates are such that gas will flow through from the cooler to the hotter side. The vanes of a typical Crookes radiometer are not porous, but the space past their edges behaves like the pores in Reynolds's plate. On average, the gas molecules move from the cold side toward the hot side whenever the pressure ratio is less than the square root of the (absolute) temperature ratio. The pressure difference causes the vane to move cold (white) side forward.

Appendix B

Iteration C code

Here the C code for the simulation, step by step, of the total number of active groups in the whole deposited ppAAc film is displayed.

There are three parameters: kill, add and pre. The parameters "kill" takes in account to systematically destroy a fixed percentage of the total groups. The "add" parameter is the amount of groups deposited every step and the "pre" parameter is the pressure factor. That is, it lowers the number of deposited groups per step, accordingly with the diminishing total pressure.

```
#include<stdio.h>
#include<stdlib.h>
#include<string.h>
// good value are add=0.04 kill=0.9998 pre=0.9994
int main(int argc,char * argv[]){
FILE *F;
int i,ref,N=8000;
double x=0,kill,add,pre;
F=fopen("out.txt","w");
for(i=0;i<N;i++){
```

```
fprintf(F,“%d %lf ”,i,x);
x=(x+add)*(kill);
add*=(pre);
fprintf(F,“%lf\n”,add);
}
fclose(F);
return 0;
}
```

Appendix C

PEG grafting

The Polyethylene glycol is a macromolecule witch structural formula is $H{-}[O{-}CH_2{-}CH_2]_n{-}OH$, where n can equal thousands of unities. It is possible to obtain PEG with particular terminal groups, for instance, amine groups. The amine group react with the carboxy group to form a covalent bond following the next reaction:
$NH_2{-}PEG{-}NH_2 + COOH \longrightarrow CONH{-}PEG{-}NH_2$.

Glossary

AAc Acrylic Acid, 17, 19, 22, 24, 26, 36, 43, 52

AFM Atomic Force Microscope, 21, 34, 36, 37, 39, 43

ATR Attenuated Total Reflectance, 20, 26, 28–30, 42

CA Contact Angle, 21, 30

FTIR Fourier Transform Infrared, 20, 28

PAA Polymerized Acrylic Acid, 14, 46

PBS Phosphate Buffer Saline, 26, 30

PECVD Plasma Enhanced Chemical Vapour Deposition, 8

PEG Poly-(Ethylene Glycol), 13, 56, 58, 65

PP Polypropylene ($[C_3H_6]_x$, 9, 12, 13, 21, 27–30, 33, 36, 39, 43, 56, 58

ppAAc plasma polymerized Acrylic Acid, 21, 29, 34, 36, 40, 42, 43, 45, 46, 56, 59, 63

RF Radio Frequency, 24, 36, 37

THA Thionin Acetate, 21, 39

VUV Vacuum Ultra Violet radiation, 6, 49, 51

XPS X-Ray Photoelectron Spectroscopy, 42, 43, 45

Contents

List of Figures

List of Tables

Bibliography

[1] F.F. Chen. *Introduction to plasma physics*. Plenum press New York, 1974.

[2] D.A. Gurnett and A. Bhattacharjee. *Introduction to Plasma Physics: With Space and Laboratory Applications*. Cambridge University Press, 2005.

[3] M Paul Bellan. *Fundamentals of Plasma Physics*. Cambridge University Press, 2006.

[4] JD Huba and D. Book. *NRL plasma formulary*, 2006.

[5] M.A. Lieberman and A.J. Lichtenberg. *Principles of plasma discharges and materials processing*. Wiley-Interscience, 2005.

[6] R. Morent, N. De Geyter, Sandra Van Vlierberghe, Els Vanderleyden, Peter Dubruel, Christophe Leys, and Etienne Schacht. Deposition of polyacrylic acid films by means of an atmospheric pressure dielectric barrier discharge. *Plasma Chemistry and Plasma Processing*, 29(2):103–117, 2009.

[7] H Yasuda and M Gazicki. Biomedical applications of plasma polymerization and plasma treatment of polymer surfaces. *Biomaterials*, 3(2):68–77, 1982.

[8] H Yasuda and Y Matsuzawa. Economical advantages of low-pressure plasma polymerization coating. *Plasma Processes and Polymers*, 2(6):507–512, JUL 2005.

[9] HK Yasuda. Some important aspects of plasma polymerization. *Plasma Processes and Polymers*, 2(4):293–304, MAY 2005.

[10] H. Yasuda and T. Hirotsu. Critical evaluation of conditions of plasma polymerization. *Journal of Polymer Science: Polymer Chemistry Edition*, 16(4), 1978.

[11] DF Williams. Progress in biomedical engineering, 1987.

[12] B.D. Ratner. New ideas in biomaterials science-a path to engineered biomaterials. *Journal of biomedical materials research*, 27(7), 1993.

[13] C. Oehr. Plasma surface modification of polymers for biomedical use. *Nuclear Inst. and Methods in Physics Research, B*, 208:40–47, 2003.

[14] P. Favia and R. D'Agostino. Plasma treatments and plasma deposition of polymers for biomedical applications. *Surface and coatings technology*, 98(1-3):1102–1106, 1998.

[15] MJ Wang, KM Liechti, Q Wang, and JM White. Self-assembled silane monolayers: Fabrication with nanoscale uniformity. *Langmuir*, 21(5):1848–1857, MAR 2005.

[16] JC Love, LA Estroff, JK Kriebel, RG Nuzzo, and GM Whitesides. Self-assembled monolayers of thiolates on metals as a form of nanotechnology. *Chemical Reviews*, 105(4):1103–1169, APR 2005.

[17] S Cosnier. Affinity biosensors based on electropolymerized films. *Electroanalysis*, 17(19):1701–1715, SEP 2005.

[18] JC Huie. Guided molecular self-assembly: a review of recent efforts. *Smart Materials and Structures*, 12(2):264–271, APR 2003.

[19] R D'Agostino, P Favia, C Oehr, and MR Wertheimer. Low-temperature plasma processing of materials: Past, present, and future. *Plasma Processes and Polymers*, 2(1):7–15, JAN 2005.

[20] Kim S. Siow, L. Britcher, S. Kumar, and H.J. Griesser. Plasma methods for the generation of chemically reactive surfaces for biomolecule immobilization and cell colonization-A review. *Plasma Processes and Polymers*, 3(6-7):392–418, 2006.

[21] N Inagaki, S Tasaka, and K Hibi. Surface modification of kapton film by plasma treatments. *Journal of Polymer Science Part A-Polymer Chemistry*, 30(7):1425–1431, JUN 1992.

[22] L O'Toole, AJ Beck, and RD Short. Characterization of plasma polymers of acrylic acid and propanoic acid. *Macromolecules*, 29(15):5172–5177, JUL 1996.

[23] DG Castner and BD Ratner. Biomedical surface science: Foundations to frontiers. *Surface Science*, 500(1-3):28–60, MAR 2002.

[24] P. Rossini, P. Colpo, G. Ceccone, KD Jandt, and F. Rossi. Surfaces engineering of polymeric films for biomedical applications. *Materials Science and Engineering C*, 23(3):353–358, 2003.

[25] MR Alexander and TM Duc. A study of the interaction of acrylic acid/1, 7-octadiene plasma deposits with water and other solvents. *Polymer-London*, 40:5479–5488, 1999.

[26] C. Brun, A. Chambaudet, C. Mavon, F. Berger, M. Fromm, and F. Jaffiol. Modifications of polypropylene surface properties by alpha ionizing radiation. *Applied Surface Science*, 157(1-2):85–91, 2000.

[27] J.M. Kelly, R.D. Short, and M.R. Alexander. Experimental evidence of a relationship between monomer plasma residence time and carboxyl group retention in acrylic acid plasma polymers. *Polymer*, 44(11):3173–3176, 2003.

[28] VB Ivanov, J. Behnisch, A. Holländer, F. Mehdorn, and H. Zimmermann. Determination of Functional Groups on Polymer Surfaces Using FluorescenceLabelling. *Surface and Interface Analysis*, 24(4):257–262, 1996.

[29] S. Zanini, R. Ziano, and C. Riccardi. Stable Poly(Acrylic Acid) Films from Acrylic Acid/Argon Plasmas: Influence of the Mixture Composition and the Reactor Geometry on the Thin Films Chemical Structures. *Plasma Chemistry and Plasma Processing*, 2009. DOI 10.1007/s11090-009-9193-z.

[30] L. Detomaso, R. Gristina, G.S. Senesi, R. dAgostino, and P. Favia. Stable plasma-deposited acrylic acid surfaces for cell culture applications. *Biomaterials*, 26(18):3831–3841, 2005.

[31] V. Sciarratta, U. Vohrer, D. Hegemann, M. Müller, and C. Oehr. Plasma functionalization of polypropylene with acrylic acid. *Surface and Coatings Technology*, 174:805–810, 2003.

[32] S. Zanini, M. Müller, C. Riccardi, and M. Orlandi. Polyethylene Glycol Grafting on Polypropylene Membranes for Anti-fouling Properties. *Plasma Chemistry and Plasma Processing*, 27(4):446–457, 2007.

[33] R. Jafari, F. Arefi-Khonsari, M. Tatoulian, D. Le Clerre, L. Talini, and F. Richard. Development of oligonucleotide microarray involving plasma polymerized acrylic acid. *Thin Solid Films*, 517(19):5763–5768, 2009.

[34] D. Hegemann and M.M. Hossain. Influence of Non-Polymerizable Gases Added During Plasma Polymerization. *Plasma Processes and Polymers*, 2(7), 2005.

[35] D. Hegemann, M.M. Hossain, E. Korner, and D.J. Balazs. Macroscopic description of plasma polymerization. *Plasma Processes and Polymers*, 4(3), 2007.

[36] S. Uchida, S. Takashima, M. Hori, M. Fukasawa, K. Ohshima, K. Nagahata, and T. Tatsumi. Plasma damage mechanisms for low-k porous SiOCH films due to radiation, radicals, and ions in the plasma etching process. *Journal of Applied Physics*, 103:073303, 2008.

[37] J.F. Friedrich, R. Mix, R.D. Schulze, A. Meyer-Plath, R. Joshi, S. Wettmarshausen, and V.D.I.T.Z.P.T. Düsseldorf. New Plasma Techniques for Polymer Surface Modification with Monotype Functional Groups. *Plasma Processes and Polymers*, 5(5):407–423, 2008.

[38] S. Zanini, C. Riccardi, S.M. Doglia, R. Ziano, A. Natalello, and A.M. Villa. Fibrinogen adsorption on plasma modified polypropylene films. *High Temperature Material Processes*, 13(3):405–412, 2009.

[39] F. Nicotra, L. Russo, N. Shaikh, L. Cipolla, S. Zanini, C. Riccardi, R. Ziano, F. Valentini, and E. Landic. Covalent Biofunctionalisation of hydroxyapatite scaffolds via plasma technology. In *22nd European Conference on Biomaterials, Lausanne, CH*, 07-11th September 2009.